Text2Loc++: Generalizing 3D Point Cloud Localization from Natural Language

Yan Xia, Letian Shi, Yilin Di, João F. Henriques, and Daniel Cremers

Abstract—We tackle the problem of localizing 3D point cloud submaps using complex and diverse natural language descriptions, and present Text2Loc++, a novel neural network designed for effective cross-modal alignment between language and point clouds in a coarse-to-fine localization pipeline. To support benchmarking, we introduce a new city-scale dataset covering both color and non-color point clouds from diverse urban scenes, and organize location descriptions into three levels of linguistic complexity. In the global place recognition stage, Text2Loc++ combines a pretrained language model with a Hierarchical Transformer with Max pooling (HTM) for sentence-level semantics, and employs an attention-based point cloud encoder for spatial understanding. We further propose Masked Instance Training (MIT) to filter out non-aligned objects and improve multimodal robustness. To enhance the embedding space, we introduce Modality-aware Hierarchical Contrastive Learning (MHCL), incorporating cross-modal, submap-, text-, and instance-level losses. In the fine localization stage, we completely remove explicit text-instance matching and design a lightweight yet powerful framework based on Prototype-based Map Cloning (PMC) and a Cascaded Cross-Attention Transformer (CCAT). Extensive experiments on the KITTI360Pose dataset show that Text2Loc++ outperforms existing methods by up to 15%. In addition, the proposed model exhibits robust generalization when evaluated on the new dataset, effectively handling complex linguistic expressions and a wide variety of urban environments. The code and dataset will be made publicly available.

Index Terms—Cross-modal Localization, Point Cloud, Autonomous Driving.

1 Introduction

3D localization [1], [2] from natural language descriptions within large-scale urban maps plays a crucial role in enabling autonomous agents to collaborate effectively with humans for trajectory planning [3]. Such capability is essential in real-world applications including goods delivery and vehicle pickup [4], [5]. In practice, tasks such as food delivery often encounter the so-called "last mile problem". Identifying the exact drop-off point within residential neighborhoods or large office complexes is particularly challenging, as GPS signals tend to degrade or fail in environments surrounded by tall buildings and dense vegetation [6], [7]. Couriers commonly rely on verbal guidance from recipients to reach the correct destination. More generally, this "last mile problem" manifests whenever users attempt to navigate to unfamiliar or occluded locations, thereby highlighting the necessity of developing localization systems that can operate directly from natural language inputs which is shown in Fig. 1.

A promising direction is to align linguistic descriptions with pre-constructed 3D point-cloud maps obtained from calibrated depth sensors such as LiDAR. Compared with image-based localization, point-cloud-based methods focus on geometric scene structures and thus offer significant

Yan Xia is with the School of Artificial Intelligence and Data Science, University of Science and Technology of China, 230026 Hefei, China (e-mail: yan.xia@ustc.edu.cn).

Letian Shi, Yilin Di, and Daniel Cremers are with Technical University of Munich, 80333 Munich, Germany (e-mail: letian.shi@tum.de, yilin.di@tum.de, cremers@tum.de).

João F. Henriques is with the Visual Geometry Group, University of Oxford, Oxford OX1 2JD, United Kingdom (e-mail: joao@robots.ox.ac.uk).

advantages: they exhibit strong robustness to changes in illumination, weather, and season, whereas the same scene captured in images may vary drastically in appearance under different environmental conditions.

However, there are four-fold challenges of 3D localization from natural language descriptions: (1) Natural language is often vague; the network must accurately capture cross-modal semantics between point clouds and texts. (2) Language and 3D data are structurally different; the network must learn to effectively align and fusion between modalities. (3) Text descriptions and submaps cannot be accurately aligned; the network must handle and reason over incomplete matches and correspondences. (4) Text styles and point cloud distributions vary widely across cities or countries; the network must robustly generalize to unseen cities/countries.

We notice that the existing methods [8]–[11] were primarily applied to simple and uniform text descriptions, where each sentence in the text typically conveys only a single piece of information, without the complexity or mixing found in everyday language. In addition, although the training and testing sets of 3D point clouds come from different areas, they are derived from the same city, sharing similar annotation strategies and stylistic characteristics. Thus, it is unclear whether existing methods can maintain consistent effectiveness when dealing with more complex and diverse text data.

To this end, we construct a new city-scale text-point cloud localization dataset that includes both real and synthetic point clouds from diverse cities and countries: SemanticKITTI, Paris_CARLA [12], Toronto3D [13], TUM City Campus [14], and Paris_Lille [15]. All point clouds are

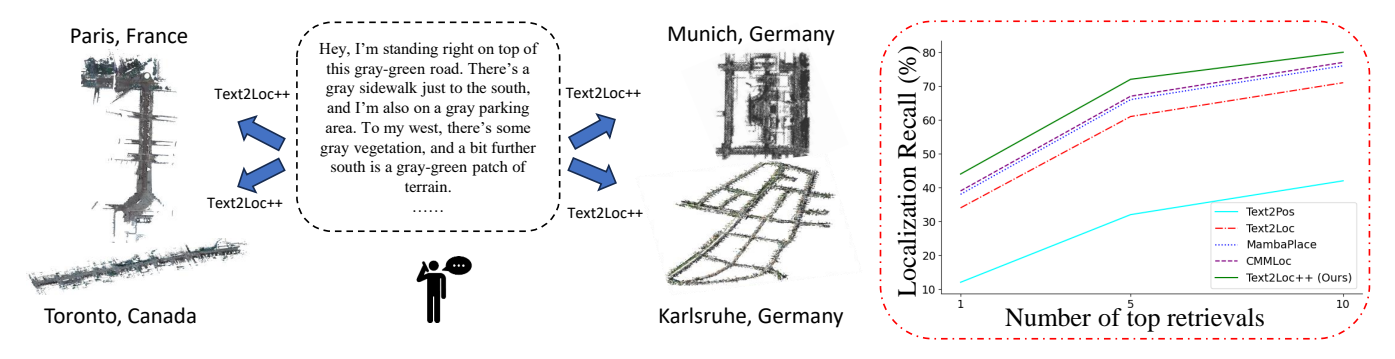


Fig. 1: (*Left*) We present Text2Loc++, a framework developed for cross-city and cross-country position localization based on textual descriptions of varying complexity. Given a 3D point cloud representing the surrounding environment and a textual query describing a location from different urban or regional contexts, Text2Loc++ identifies the most probable position corresponding to the description within the map. The model demonstrates strong generalization across diverse language inputs and heterogeneous point cloud data. (*Right*) Localization results on the KITTI360Pose test set show that the proposed Text2Loc++ consistently outperforms existing baselines across all top-k retrieval thresholds, achieving up to 15% higher accuracy in localizing text queries within a 5 m error range.

annotated following the protocol of [8]. Besides, we generate varying levels of linguistic complexity while preserving semantic consistency to describe the locations, creating a more challenging and realistic benchmark for text–point cloud localization task.

Building upon this new dataset, we revisit the fundamental challenges of text-point cloud localization. To address Challenges (1) and (2), we emphasize the necessity of effectively capturing relational dynamics among 3D instances within submaps to obtain more discriminative geometric representations. Meanwhile, textual descriptions exhibit an inherent hierarchical structure—comprising sentences and word tokens—which motivates the analysis of both intra-text (within-sentence) and inter-text (crosssentence) relationships. To this end, we employ a frozen pretrained large language model, T5 [16], and design a hierarchical transformer equipped with max-pooling to serve as an intra- and inter-text encoder. Furthermore, we extend the instance encoder from Text2Pose [8] by incorporating a number encoder and applying contrastive learning to preserve balance between positive and negative pairs.

Another key observation concerns the fine localization stage: the text-instance matching modules used in previous approaches can introduce severe noise due to inaccurate correspondence or offset predictions, thereby hindering precise position estimation. To mitigate this issue, we propose a novel matching-free fine localization network. Specifically, a prototype-based map cloning (PMC) module is designed to enrich the diversity of retrieved submaps, followed by a cascaded cross-attention transformer (CCAT) that integrates semantic information from point clouds into the text embedding. Together, these components facilitate end-to-end training, allowing for the direct prediction of the target position without relying on any text-instance matcher.

More importantly, we observe existing methods largely overlook Challenges (3) and (4). In practice, it is often infeasible to describe all instances within a 3D submap using a single textual description. Conversely, a single language description may correspond to multiple submaps that match the described scene. To handle this ambiguity, we propose

masking out non-aligned instances during training, ensuring that the model focuses only on text-relevant content. Inspired by [17] and [18], we further enhance training by proposing Modality-aware Hierarchical Contrastive Learning (MHCL), which encourages a more structured and semantically meaningful embedding space. In addition to the standard cross-modal contrastive loss, we introduce submap-level, text-level, and instance-level losses. This diverse set of objectives enables more effective representation learning, significantly improving the robustness and generalization of the model without sacrificing accuracy.

To better handle complex and diverse textual descriptions, we introduce a new training strategy to enhance the model's language understanding and cross-modal alignment capabilities. Specifically, we adopt the LoRA approach [19] to fine-tune the T5 encoder, enabling the model to extract semantic information from natural language inputs more effectively. However, as text complexity increases, direct alignment of rich language descriptions with point clouds becomes increasingly challenging. Due to the incomplete alignment between the visible 3D content and the textual input, establishing accurate cross-modal correspondences is difficult, especially under a powerful yet unconstrained T5 encoder. To address this, we incorporate text distillation [20], which filters out irrelevant content and preserves only the most semantically salient information. This distilled representation improves the accuracy and robustness of multimodal matching.

To summarize, the main contributions of this work are:

- We focus on the relatively-understudied problem of point cloud localization from textual descriptions, to address the "last mile problem". We introduce a new benchmark for text-to-point cloud localization with multi-level linguistic complexity and both color and non-color point clouds from diverse real-world cities.
- We propose a novel attention-based method that is hierarchical and represents contextual details within and across sentence descriptions of places. We also propose a novel attention-based point cloud module.

- To address the ambiguity caused by non-aligned instances, we propose a Masked Instance Training strategy that selectively filters out irrelevant objects during training.
- To better organize the multimodal representation space, we introduce Modality-aware Hierarchical Contrastive Learning, incorporating cross-modal, submap-, text-, and instance-level losses.
- We are the first to completely remove the usage of the text-instance matcher in the final localization stage. We propose a lightweight and faster localization model that achieves state-of-the-art performance through our designed prototype-based map cloning (PMC) module in training and the cascaded crossattention transformer (CCAT).

This journal article builds upon and extends our earlier conference paper presented at CVPR 2024 [21]. In this updated version, we introduce the following extension: I) We construct a new city-scale text-point cloud localization dataset using real and synthetic point clouds from diverse urban environments. Each location is described with semantically consistent texts of varying linguistic complexity, enabling more realistic and challenging benchmarking. II) We propose a modality-aware hierarchical contrastive learning with a masked instance training strategy to address the challenge of partial matching, effectively reducing incorrect associations between modalities and boosting the robustness among different benchmarks. III) We employ LoRA and text distillation to address the challenges posed by increasing text complexity and diversity. IV) We conduct extensive experiments on the new benchmark and show that the proposed Text2Loc++ greatly improves over the state-ofthe-art methods.

2 RELATED WORK

In prior research, only a limited number of networks have been proposed for natural language–based 3D localization in large-scale outdoor environments. Closely related research areas include 2D visual localization, 3D point cloud–based localization, and language-grounded 3D understanding.

2D visual localization. 2D visual localization plays a crucial role in applications such as robotics and augmented reality, where the goal is to estimate the camera pose from a given query image or image sequence. One of the earliest approaches, Scale-Invariant Feature Transform (SIFT) [22], introduces distinctive invariant features that enable reliable object matching across viewpoints, laying the foundation for modern localization systems. Later, Oriented FAST and Rotated BRIEF (ORB) [23] improved robustness against scale, rotation, and illumination variations. Recent learningbased approaches [24], [25] typically adopt a coarse-to-fine pipeline. In the coarse stage, place recognition is performed via nearest-neighbor search in a high-dimensional embedding space. The fine stage establishes pixel-wise correspondences between the query and retrieved reference images to refine the pose estimation. Despite their success, these image-based methods often experience significant performance drops under strong appearance changes caused by lighting, weather, or seasonal variations. In contrast to 2D

feature matching, our work focuses on cross-modal localization—predicting 3D positions based on textual queries and 3D point clouds.

3D point cloud based localization. Driven by progress in image-based localization, deep learning for 3D localization has become an active research field. Similar to image-based systems, most methods follow a two-stage design: (1) place recognition, and (2) pose estimation. Point-NetVlad [26] is a pioneering network enabling end-toend learning for 3D place recognition. Building upon this, SOE-Net [27] introduces the PointOE module, integrating orientation encoding into PointNet to produce point-wise local descriptors. Many subsequent studies [28]-[34] explore transformer-based architectures with stacked self-attention blocks to capture long-range dependencies and contextual features. Alternatively, MinkLoc3D [35] employs a voxelbased strategy to produce a compact global descriptor using a Feature Pyramid Network (FPN) [36] and generalizedmean (GeM) pooling [37]. However, voxelization inherently causes quantization errors and point loss. To mitigate this, CASSPR [6] introduces a dual-branch hierarchical crossattention transformer, combining the strengths of voxelbased and point-based representations. Once the coarse location is determined, pose estimation can be refined using point cloud registration algorithms, such as Iterative Closest Point (ICP) [38] or autoencoder-based registration [39]. Unlike conventional geometric methods, our approach employs natural language descriptions to identify and localize arbitrary target positions in 3D space.

3D vision and language. The integration of 3D vision and natural language has recently drawn increasing research interest. Prabhudesai et al. [40] implicitly link language to 3D visual feature representations to predict objectlevel 3D bounding boxes. Other methods [41]–[44] perform referential grounding, locating the most relevant 3D objects within a scene from textual descriptions. However, these approaches primarily focus on indoor environments. Text2Pos [8] represents the first attempt at large-scale outdoor localization using natural language. It identifies coarse candidate locations and refines the pose estimation in a subsequent stage. Following this, Wang et al. [9] introduce a Transformer-based framework to enhance representation discriminability for both point clouds and text queries. More recently, MambaPlace [10] and CMMLoc [11] further push performance boundaries by integrating advanced sequence modeling techniques, namely the Mamba and Cauchy Mix modules, respectively.

3 Problem Statement

We define a large-scale 3D reference map as

$$M_{\text{ref}} = \{ s_i \mid i = 1, \dots, M \},\$$

where each cubic submap s_i is a set of 3D object instances

$$s_i = \{ p_i^j \mid j = 1, \dots, n_{s_i} \},\$$

and n_{s_i} denotes the number of instances in s_i . Let $\{t_i \mid i=1,\ldots,M'\}$ be the collection of text descriptions; each description t_i consists of spatial hints $\{h_i^k\}_{k=1}^{n_h}$, where each h_i^k specifies a relation between the target location and an

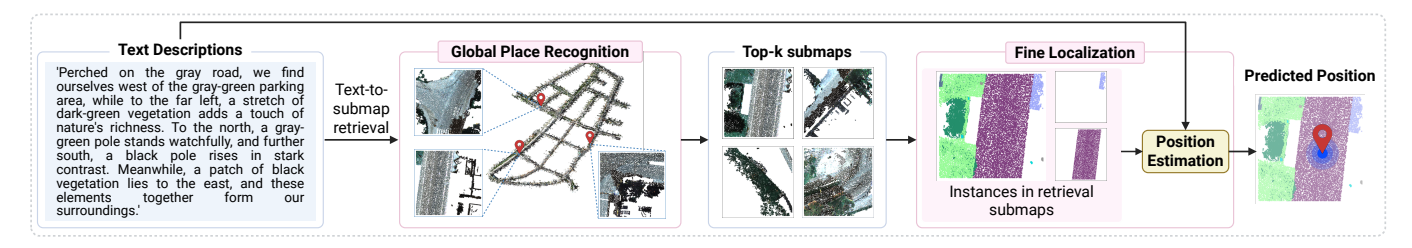


Fig. 2: The proposed Text2Loc++ architecture. It consists of two tandem modules: Global place recognition and Fine localization. *Global place recognition*. Given a text-based position description, we first identify a set of coarse candidate locations, "submaps," potentially containing the target position. This is achieved by retrieving the top-k nearest submaps from a previously constructed database of submaps using our novel text-to-submap retrieval model. *Fine localization*. We then refine the center coordinates of the retrieved submaps via our designed matching-free position estimation module, which adjusts the target location to increase accuracy.

object instance. (M and M' is the number of 3D reference map and text descriptions)

Following [8], we adopt a two-stage *coarse-to-fine* scheme. In the coarse stage (text–submap global place recognition), a function F jointly encodes a text description t and a submap $s \in M_{\rm ref}$ into a shared embedding space, such that matched text–submap pairs are pulled together while unmatched pairs are pushed apart. In the fine stage, a matching-free network directly regresses the target position from the text and the retrieved submaps.

Accordingly, learning language-guided 3D localization reduces to predicting the ground-truth planar coordinates (x, y) (with respect to the scene frame) via

$$\min_{\phi, F} \mathbb{E}_{(x,y,t) \sim \mathcal{D}} \left\| (x,y) - \phi \left(t, \underset{s \in M_{\text{ref}}}{\operatorname{argmin}} \ d \left(F(t), F(s) \right) \right) \right\|^{2}, (1)$$

where $d(\cdot,\cdot)$ is a distance metric (e.g., Euclidean), $\mathcal D$ denotes the dataset, and ϕ maps a text description and a submap to fine-grained coordinates from a text description t and a submap s.

4 METHODOLOGY

Fig. 2 shows our Text2Loc++ architecture. To accomplish text-to-submap retrieval, we employ separate text and submap branches to extract modality-specific features. A masked instance modality-aware contrastive learning framework is then used to train the model for precise multimodal alignment. Additionally, to cope with varying levels of textual complexity, we introduce a text distillation mechanism. These components, described in Section 4.1, enable Text2Loc++ to adapt not only to varying levels of textual input complexity, but also to diverse urban environments and point cloud configurations, allowing it to retrieve a set of candidate submaps that potentially contain the target location. Subsequently, the retrieved submaps are utilized to refine the estimated position via a specifically designed fine localization module, detailed in Section. 4.2.

4.1 Global Place Recognition

3D point cloud based place recognition is formulated as a retrieval problem, in which the task is to identify the most similar reference scan and its corresponding spatial location for a given query LiDAR scan. This is typically achieved by comparing the query's global descriptor with those extracted from a database of reference scans, where the similarity is measured using a predefined descriptor distance metric. Building on this paradigm, we extend the concept to a text-submap cross-modal global place recognition framework for coarse localization. In this setting, the objective is to retrieve the submap that best corresponds to a natural language description. The key challenge lies in learning global descriptors for 3D submaps S and textual queries T that are both robust to modality-specific variations and discriminative enough to distinguish fine-grained spatial contexts. Following prior works [8], [9], we employ a dual-branch encoding architecture that maps submaps S and textual descriptions T into a shared embedding space, as depicted in Fig. 3 (left).

Text Branch. We begin by utilizing a frozen, pre-trained large language model (T5) [16] to extract fine-grained semantic representations from textual descriptions, thereby improving the quality of text embeddings. To further capture contextual dependencies, we design a hierarchical transformer architecture equipped with max-pooling layers. This module models both intra-sentence relationships through self-attention and inter-sentence semantics by aggregating information shared across sentences, as illustrated in Fig. 3 (right bottom). The transformer serves as our intraand inter-text encoder, where each block is implemented as a residual module consisting of Multi-Head Self-Attention (MHSA) and Feed-Forward Network (FFN) sublayers. The FFN comprises two linear layers activated by ReLU. Additional architectural details are provided in the Supplementary Material.

3D Submap Branch. Each instance P_i in the submap S_N is represented as a point cloud that has both spatial and color (RGB) coordinates, forming the 6D features* (Fig. 3 (right top)). To extract semantic features from these points, we employ the most efficient 3D encoder - PointNet++ [45], though any more advanced encoder could be substituted. In parallel, we generate a color embedding by encoding RGB values using a color encoder and a positional embedding by encoding the instance centroid \bar{P}_i (i.e., the mean coordinates) through a positional encoder. Since different object instances typically contain varying numbers of points(for example, road surfaces usually have more than 1,000 points, whereas poles have fewer than 500), we introduce a num-

*. The 6D-feature input is for the point cloud with color. If the point cloud is without color information, we only include x-y-z coordinates.

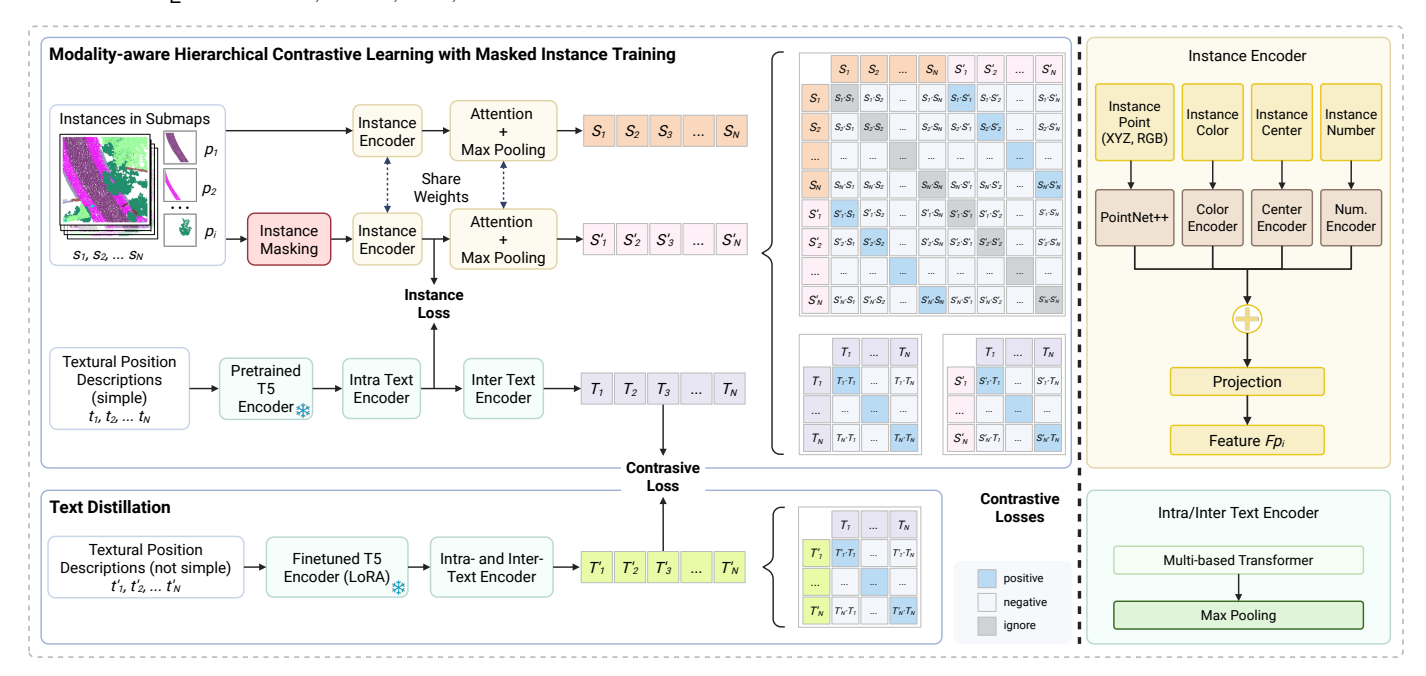


Fig. 3: (*left*) The architecture of global place recognition and the training procedure in the global place recognition. (*right*) The architecture of instance encoder as well as intra/inter-text encoder architecture for point clouds. Note that the pre-trained/finetuned T5 model is frozen.

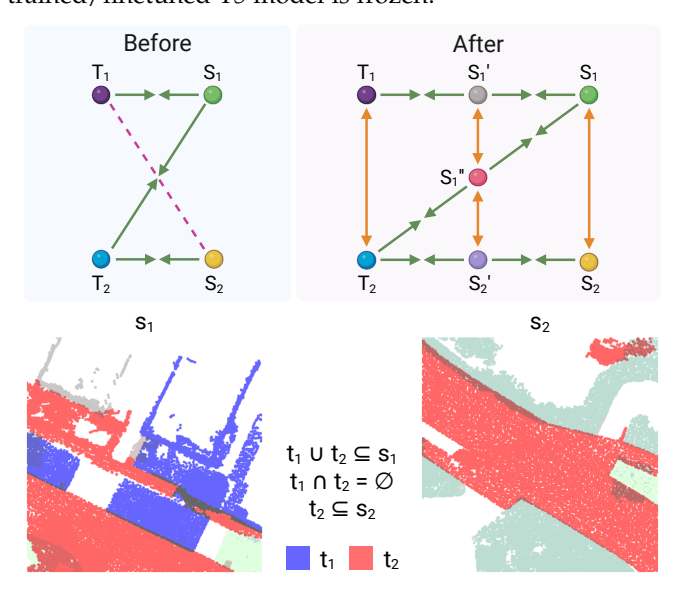


Fig. 4: (top) Comparison for without and with masked instance modality-aware hierarchical contrastive learning in the training process. T_1 and T_2 are different text embeddings. S_1 and S_2 are different submap embeddings from s_1 and s_2 . S_1' , S_1'' , and S_2' are submap embeddings with masked instance process. (bottom) Illustration of the text-instance relationship. t_1 and t_2 not only represent the text but also stand for the instances described by the respective text. In submap s_1 and s_2 , the blue and red area stands for the instances t_1 and t_2 .

ber encoder to explicitly represent this variation. Encoding the point count provides a useful class-specific prior that enhances instance differentiation. All encoders (color, positional, and number) are implemented as three-layer multilayer perceptrons (MLPs), producing feature vectors with dimensions aligned to the semantic point embeddings. The resulting semantic, color, positional, and numerical

embeddings are concatenated and passed through a projection layer—another three-layer MLP—that outputs the final instance embedding F_{p_i} . Finally, the set of *in-submap* instance descriptors $\{F_{p_i}\}_{i=1}^{N_p}$ is aggregated into a global submap descriptor F^S using an attention layer [27] followed by a max pooling operation.

Masked Instance Training. Point clouds contain detailed and structured spatial information, whereas language is inherently unstructured and context-dependent. This modality gap introduces ambiguity, where a single submap may correspond to various textual descriptions, and a single text may match multiple submaps based on interpretation. As shown in Fig. 4, $T_i = F(t_i), (i = 1, 2)$ and $S_i = F(s_i), (i = 1, 2)$ are text and submap embeddings, respectively. The definitions for t_i and s_i are in Section ??. This example highlights the issue discussed above: the submap s_1 matches both the textual descriptions t_1 and t_2 , while t_2 also corresponds to both s_1 and s_2 . When applying standard contrastive learning, the model is incorrectly encouraged to pull T_1 closer to S_2 , introducing semantic inconsistency. This illustrates a fundamental limitation of naive contrastive objectives in the presence of many-to-many cross-modal correspondences.

To address this issue, we propose a novel Masked Instance Training (MIT) strategy. Specifically, each submap is defined as $s_i = s_i^l \cup s_i^{nl}$, where s_i^l denotes the set of instances described in the text, and s_i^{nl} includes those that are not. During training, we randomly sample a subset $s_i^{'nl} \subseteq s_i^{nl}$ and construct a masked submap $s_i' = s_i^l \cup s_i^{'nl}$. This encourages the model to focus on semantically aligned content while being robust to irrelevant or noisy instances. A detailed algorithmic description is provided in the Supplementary Material. The proposed MIT improves the alignment of the cross-modal under many-to-many matching conditions, as validated by Ablation Studies.

Modality-aware Hierarchical Contrastive Learning. In-

spired by CLIP [46], we compute the feature distance between textual descriptions and 3D point cloud. Given an input batch of 3D submap descriptors $\{S_i\}_{i=1}^N$ and matching text descriptors $\{T_i\}_{i=1}^N$ where N is the batch size. We utilize the proposed masked instance training strategy to generate the 3D submap descriptors $\{S_i'\}_{i=1}^N$, which include only part of the instances in certain submaps. The heterogeneous contrastive loss among each pair is computed as follows.

$$l(i, T, S') = -\log \frac{\exp(T_i \cdot S_i'/\tau)}{\sum_{j \in N} exp(T_i \cdot S_j'/\tau)} - \log \frac{\exp(S_i' \cdot T_i/\tau)}{\sum_{j \in N} \exp(S_i' \cdot T_j/\tau)}, \quad (2)$$

where τ is the temperature coefficient, similar to CLIP [46]. Within a training mini-batch, the text-submap alignment objective can be described as:

$$L_{\text{cross-modal}} = L(T, S') = \frac{1}{N} \left[\sum_{i \in N} l(i, T, S') \right]. \tag{3}$$

As discussed in the last section, text-to-submap matching inherently exhibits a many-to-many correspondence, making it difficult to establish precise alignments between textual descriptions and point cloud data; consequently, constraining solely at the submap level proves inadequate for capturing fine-grained cross-modal relationships. Thus, we incorporate an instance-level loss to constrain the alignment between text embeddings and the corresponding instance embeddings within the submap. Given an input batch of 3D instance descriptors $\{I_i^S\}_{i=1}^{N_I}$ and matching text descriptors $\{I_i^T\}_{i=1}^{N_I}$ with the instance where M is the number of the number of the instance. For simplicity, we take a fixed number of instances in each batch $N_I = kN(k \in \mathbb{N}^+)$.

$$L_{\text{inst}} = L(I^T, I^S) = \frac{1}{N_I} \left[\sum_{j \in M} l(j, I^T, I^S) \right].$$
 (4)

To address the limitations illustrated in Fig. 4, we aim to construct a semantically meaningful embedding space that requires not only cross-modal supervision but also modality-aware constraints. For text embeddings, it is essential that distinct descriptions are mapped to well-separated regions in the embedding space. To enforce this, we introduce a text contrastive loss that explicitly encourages inter-text separation. For submap embeddings, our goal is twofold: (1) ensure sufficient separation between embeddings of different submaps, and (2) maintain consistency between each submap and its masked variants, which share the same semantic description and should thus remain close despite perturbations. To jointly enforce these objectives, we propose a double contrastive learning framework that penalizes mismatched submap-masked submap pairs while promoting alignment across multiple representations of the same semantic content.

$$l_d(i, S, S') = -\log \frac{\exp(S_i \cdot S_i'/\tau)}{\sum\limits_{j \in N} \exp(S_i \cdot S_j'/\tau) + \sum\limits_{\substack{j \in N \\ j \neq i}} \exp(S_i' \cdot S_j'/\tau)}$$
$$-\log \frac{\exp(S_i' \cdot S_i/\tau)}{\sum\limits_{\substack{j \in N \\ j \neq i}} \exp(S_i' \cdot S_j/\tau) + \sum\limits_{\substack{j \in N \\ j \neq i}} \exp(S_i \cdot S_j/\tau)}$$
(5)

We define the text, and the submap, and the final loss loss below.

$$L_{\text{text}} = L(T, T) = \frac{1}{N} \left[\sum_{i \in N} l(i, T, T) \right]. \tag{6}$$

$$L_{\text{submap}} = L(S', S) = \frac{1}{N} \left[\sum_{i \in N} l_d(i, S', S) \right]. \tag{7}$$

$$L = \alpha_1 L_{\text{cross-modal}} + \alpha_2 L_{\text{inst}} + \alpha_3 L_{\text{submap}} + \alpha_4 L_{\text{text}}.$$
 (8)

After applying masked instance modality-aware hierarchical contrastive learning, the training process is illustrated in Fig. 4 (top right).

Text Distillation. As textual descriptions increase in complexity, the modality gap between language and point cloud data, along with the model's limited capacity to simultaneously extract fine-grained semantics and perform accurate cross-modal alignment, renders direct matching ineffective. To mitigate this challenge, we propose a stepwise training strategy based on text distillation, which progressively guides the model toward robust understanding and alignment of complex linguistic inputs with 3D spatial representations First, we perform multimodal contrastive learning between simple descriptions and point clouds. Then, we freeze the previously trained network and introduce a new text module to handle moderate or complex text descriptions, generating new text embeddings. Since the original pretrained T5 module is no longer effective in processing complex text, we finetune the T5 encoder using the LoRA approach [19]. The detail finetune steps are in the supplementary. For content-equivalent simple text descriptions, we use the original frozen text module to produce the old text embeddings. In the embedding space, these two embeddings should be close to each other due to their shared text meaning, so we apply a contrastive learning loss between them. A more thorough comparative study is in Section 6.3.

4.2 Fine Localization

Following the text–submap global place recognition stage, our objective in fine localization is to refine the predicted target position within the retrieved submaps. While prior approaches [8], [9] have achieved promising results using text–submap matching strategies, the inherent ambiguity of natural language descriptions often leads to unreliable offset predictions for individual object instances. To overcome this limitation, we introduce a matching-free fine localization network, as illustrated in Fig. 5.

In this framework (Fig. 5 top), the text branch (bottom) extracts fine-grained linguistic features using a frozen or fine-tuned pre-trained language model, T5 [16], followed by an attention module and a max-pooling operation. The submap branch (top) employs a prototype-based map cloning (PMC) module to enrich the diversity of submap variants and then extracts point cloud features using the same instance encoder utilized in the global place recognition stage. Subsequently, the text and submap features are integrated through a Cascaded Cross-Attention Transformer (CCAT), after which a lightweight multi layer perceptron (MLP) regresses the final target position.

Cascaded Cross-attention Transformer (CCAT). To effectively model the interactions between the text and 3D

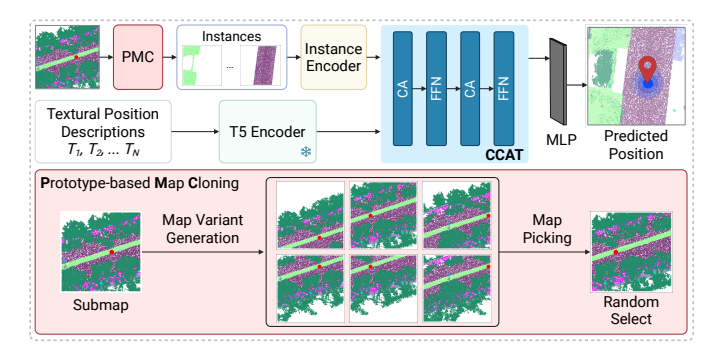


Fig. 5: (top) The proposed matching-free fine localization architecture. It consists of two parallel branches: instance encoder as the top branch and text encoder as the bottom branch. Cascaded Cross-Attention Transformers (CCAT) fuse the multimodal information. (bottom) The procedure of the Prototype-based Map Cloning (PMC).

submap branches, we introduce a Cascaded Cross-Attention Transformer (CCAT) for multimodal feature fusion. Following the design of [6], the CCAT is composed of two sequential Cross-Attention Transformer (CAT) modules, each contains a cross attention module (CA) and a feed-forward network (FFN).

In the first CA, the point cloud features serve as the Query, while the text features act as the Key and Value. This allows the model to refine the point representations by incorporating semantic cues from the text, yielding text-informed point feature maps. Conversely, in the second CA, the text features are used as the Query, and the enhanced point features from the first CAT are used as the Key and Value, resulting in text features enriched with geometric context.

Unlike the hierarchical structure proposed in [6], our design employs a cascaded configuration of the first and the second CAT, enabling progressive cross-modal interaction. In this work, we utilize two stacked CCAT blocks to achieve more comprehensive feature fusion. Further ablation studies and analyses are provided in the Supplementary Material.

Prototype-based Map Cloning (PMC). To generate more diverse and informative submap variants for training, we introduce a Prototype-based Map Cloning (PMC) module in the training time. For each pair $\{t_i, s_i\}$, our goal is to construct a collection of neighboring submap variants \mathcal{G}_i centered around the current map S_i , which can be formulated as follows:

$$\mathcal{G}_i = \{ S_j \mid \left\| \bar{s}_j - \bar{s}_i \right\|_{\infty} < \alpha, \ \left\| \bar{s}_j - c_i \right\|_{\infty} < \beta \}, \tag{9}$$

where $\bar{s_i}$, $\bar{s_j}$ are the center coordinates of the submaps s_i and s_j respectively. c_i represents the ground-truth target position described by t_i , α and β are the pre-defined thresholds.

In practice, we observe that certain submaps in \mathcal{G}_i don't have enough object instances corresponding to the textual descriptions T_i . To mitigate this issue, we apply a filtering procedure by enforcing a minimum instance threshold, allowing at most N_m instance mismatch. After this filtering step, a single submap is randomly sampled from the refined \mathcal{G}_i for training.

Loss function. In contrast to previous approaches [8], [9], our fine localization network eliminates the text–instance matching module, resulting in a simpler and more efficient training process. It is important to note that this network is trained independently from the global place recognition stage. The objective of training is to minimize the distance between the predicted target position and the ground truth. To this end, we employ a mean squared error loss L_r as the sole optimization objective for the translation regressor.

$$L(C_{qt}, C_{pred}) = ||C_{qt} - C_{pred}||_{2},$$
 (10)

where $C_{pred} = (x, y)$ (see Eq. (1)) is the predicted target coordinates, and C_{gt} is the ground-truth coordinates.

5 EXPERIMENTS

5.1 Experimental Datasets

The KITTI-360 dataset offers a large number of scenes with notable geographic and point cloud variations between training and testing sets. However, all data are collected in the same city using the same LiDAR device, and each pose is precisely georegistered in OpenMap, resulting in a high level of consistency. Therefore, to evaluate a model's generalization capability, it must maintain stable performance across diverse cities, devices, and acquisition settings. To this end, we incorporate more varied data sources to evaluate robustness and generalization.

We train and evaluate the proposed Text2Loc++ on six benchmark datasets designed for text-based point cloud localization. This includes the two KITTI360Pose benchmarks [8] and four additional datasets containing point clouds with semantic annotations: Toronto [13], Paris_CARLA [12], TUM [14], and Paris_Lille [15]. The two KITTI360Pose datasets share identical submap structures and textual descriptions; the only distinction lies in the presence or absence of color information in the point clouds. Specifically, the Toronto and Paris_CARLA datasets provide colored point clouds, whereas the TUM and Paris_Lille datasets contain only geometric data and semantic annotations. With the exception of the KITTI360Pose dataset, we augment all point clouds with textual descriptions according to the protocol proposed in [8]. Additionally, we standardize semantic labels across all datasets to ensure consistency in representation across different urban environments.

5.1.1 Data Specification

Except from Kitti360, the other datasets offer annotated point clouds collected from urban environments with different schemes of semantic categories. We visualize the new submaps generated by ourselves in Fig. 6. For Toronto and TUM datasets, they only have 8 raw semantic categories. Thus, we follow the semantic class definition in KITTI360 [47] to split and annotate the point clouds. Since we only focus on the layout of the environment, the dynamic objects are removed from the raw point clouds. For Paris_CARLA and Paris_Lille datasets, we directly convert the label if the name of the category exists in the KITTI360 class definition. If not, we utilize the class definition in [48]. Then, the submaps and texts are created in the same way of KITTI360Pose. In detail, the 3D submap is a cube that

		Baseline			Refinement				
Dataset Color		Training		Testing		Training		Testing	
		# submaps	# texts	# submaps	# texts	# submaps	# texts	# submaps	# texts
Kitti360 Paris_CARLA Toronto	✓ ✓ ✓	11259 - -	28807 - -	4308 1004 685	11505 3857 2087	11259 2936 -	28807 10855 -	4308 1004 685	11505 3857 2087
Kitti360 (no color) Paris_Lille TUM	X X X	11259 - -	28807 - -	4308 185 183	11505 845 755	11259 566 350	28807 2337 1518	4308 185 183	11505 845 755

TABLE 1: Dataset information. Number of training and testing submaps and texts for our baseline and refinement networks. Color means whether the point cloud contains color information.

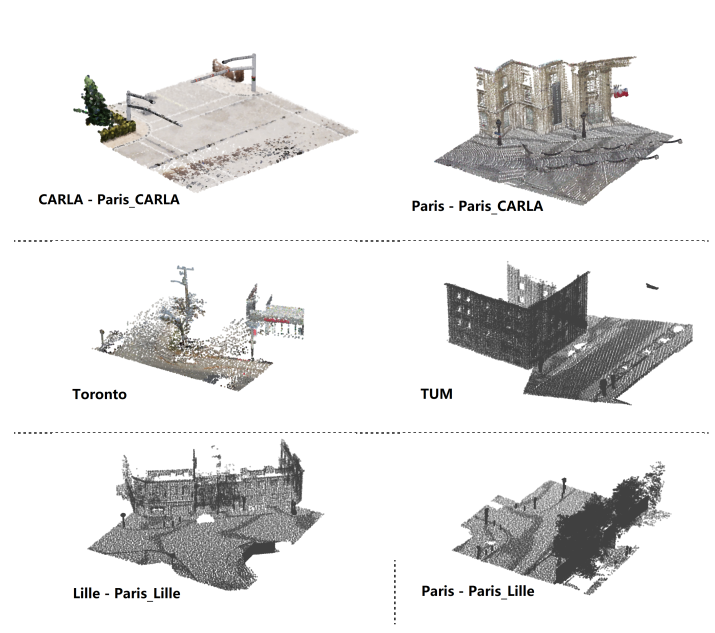


Fig. 6: Samples of point cloud from different datasets. We present visualizations of the point clouds from the four constructed benchmark datasets. Subfigures CARLA - Paris_CARLA, Paris - Paris_CARLA, and Toronto depict datasets with color information, whereas other subfigures correspond to datasets without color attributes.

is 30m long with a stride of 10m. Below are the detailed explanations for each dataset:

KITTI360Pose Dataset. We use the dataset constructed by [8], which consists of point clouds from 9 districts, covering 43,381 position-query pairs over a total area of 15.51 km^2 . Following [8], we select five scenes (11.59 km^2) for training, one for validation, and the remaining three scenes (2.14 km^2) for testing. This results in 11,259 training submaps and 4,308 testing submaps, with a total of 15,567 submaps across the entire dataset.

Paris_CARLA Dataset is a collection of dense, colored point clouds captured in outdoor environments using a mobile platform equipped with a tilted Velodyne HDL-32 LiDAR (45° to the horizon) and a 360° Ladybug5 camera system (comprising 6 lenses). The dataset consists of two parts: a synthetic set generated with the open-source CARLA simulator (700 M points), and a real-world set collected in central Paris (60 M points). The synthetic portion covers

approximately $5.8\,\mathrm{km}$ of driving distance, while the real-world data spans $550\,\mathrm{m}$ across three streets in Paris. All data are annotated with 23 semantic classes and instance-level labels, consistent with the class definitions used in CARLA to ensure label alignment between synthetic and real domains.

Toronto Dataset. Toronto is a large-scale outdoor urban point cloud dataset collected in Toronto, Canada, using a vehicle-mounted mobile LiDAR scanning (MLS) system. The platform is equipped with a 32-line LiDAR sensor, a Ladybug5 panoramic camera, a GNSS system, and a SLAM module. Natural RGB colors are assigned to each point using camera projections. The dataset spans approximately 1 km of road and contains 78.3 million points, with UTM coordinates centered at (43.726, –79.417). All points are labeled with one of eight semantic classes.

TUM Dataset is a mobile laser-scanning dataset covering approximately $80,000\ m^2$ with detailed semantic annotations. Collected by the Fraunhofer Institute of Optronics, System Technologies, and Image Exploitation (IOSB) using two Velodyne HDL-64E laser scanners, the dataset was later annotated by the Chair of Photogrammetry and Remote Sensing at TUM. It encompasses an urban area with around $1\ \mathrm{km}$ of roadways and includes over $40\ \mathrm{million}$ annotated points, categorized into eight object classes. Notably, this dataset does not contain any images.

Paris_Lille Dataset is a mobile LiDAR dataset collected using a Velodyne HDL-32E sensor. The dataset includes point clouds from two cities—Paris and Lille—covering nearly 2 km and totaling over 140 million points. All points are annotated with fine-grained semantic labels across 50 classes.

5.1.2 Dataset Splitting

We adopt dataset-specific splitting strategies tailored to the structural characteristics of each benchmark. For datasets containing multiple traversals of the same region (e.g., KITTI360Pose, CARLA in Paris_CARLA, and Paris_Lille), training and testing reference maps are constructed from disjoint runs to ensure route-level separation. For datasets comprising only a single traversal, alternative protocols are employed: the entire Toronto dataset is reserved for evaluation, whereas in Paris in Paris_CARLA and TUM, geographically distinct regions are partitioned into training and testing subsets.

Each reference map is subsequently partitioned into submaps at fixed spatial intervals along the trajectory to

Submap	KITTI360Pose	KITTI360Pose (no color)
Simple	The pose is on-top of a green vegetation. The pose is east of a dark-green fence. The pose is north of a green sidewalk. The pose is south of a green building. The pose is north of a green terrain. The pose is north of a green vegetation.	The pose is on-top of a road. The pose is east of a sidewalk. The pose is east of a vegetation. The pose is east of a fence. The pose is east of a terrain. The pose is west of a sidewalk.
Moderate	Two vegetations, the sidewalk, the building and the terrain are green. One vegetation is below the pose. The sidewalk, the terrain and one vegetation are south of the pose. The building is north of the pose. They are east of the dark-green fence.	The road is below the pose. There are two sidewalks. They are on-top of one. They are west of one. The vegetation is west of the spot. The fence ane the terrain is west of the position.
Complex	In the landscape, two areas of vegetation, the sidewalk, the building, and the surrounding terrain display a vibrant green hue, contributing to the overall vitality of the scene. One patch of greenery is situated directly below the post, while the sidewalk, the terrain, and another clump of vegetation stretch out to the south of it. Meanwhile, the building stands to the north of the post, commanding attention within the layout. All these elements are positioned east of a dark-green fence, which serves as a contrasting boundary, framing the lively environment	Beneath the pose lies a road flanked by two sidewalks, which extend above it. To the west of this location, a diverse array of vegetation thrives, accompanied by a sturdy fence that also stands in the same direction. Additionally, the terrain itself unfolds to the west, creating a cohesive landscape that defines the area surrounding this central point.

TABLE 2: Textual descriptions of the same location in the submap at different levels of linguistic complexity. Pictures are semantic bird-eye-view map for the submap with the target as red point. The left one is the text descriptions for color point cloud while the right one is for no color point cloud. The simple, moderate, and complex text descriptions each describe the same spatial relationships between the target and instances within the submap, differing only in their level of linguistic complexity.

facilitate fine-grained correspondence. Additional implementation details concerning the segmentation procedure are provided in the supplementary material.

To evaluate cross-dataset generalization, we define two training paradigms: a baseline model, trained solely on the KITTI360Pose dataset, and a refinement model, trained jointly on KITTI360Pose and supplementary datasets. Table 1 summarizes the number of training and testing submaps used for the baseline and refinement networks.

5.1.3 Textual Descriptions

In real-world communication, humans naturally describe self-locations by referencing multiple objects, their spatial relationships, and relevant attributes. In the prior publications, a text-to-point cloud system trained solely on minimal statements (e.g., 'the pose is on top of a gray road.'). This may struggle to capture the richness and nuance of human descriptions. By incorporating more complex narratives, where multiple elements and their relationships are mentioned, the model can develop a deeper, more humanlike understanding of locations. It learns to handle a wide range of linguistic expressions, from concise descriptions to detailed explanations (potentially containing redundant information), enabling it to process a broader spectrum of

user queries. This not only improves the alignment between text and 3D geometry but also supports more natural and conversational interactions. To systematically study the effect of text complexity on localization accuracy, we thus categorize text descriptions into three levels of complexity:

Simple: Each sentence describes only the spatial relationship between the self-localized target and a single reference instance, with no inter-sentence connections.

Moderate: Building on the simple level, additional attributes such as direction, color, and instance labels are integrated, resulting in more concise and human-like descriptions. Moderate inter-sentence correlations are introduced.

Complex: Extending the moderate level, sentences are further diversified to resemble real-world text or speech-to-text outputs generated by large language models (LLMs) [49]. In this setting, descriptions may contain missing details such as omitted colors or instance labels, making the text more natural but also noisier.

Table. 2 shows the distinct characteristics across different complexity levels. Detailed generation procedures are provided in the supplementary material.

					Submap	Retrieval Re	ecall (%) ↑			
Setting	Method		Simple			Moderate			Complex	
		k=1	k=3	k=5	k=1	k=3	k=5	k=1	k=3	k=5
				KITTI360	Pose [8]					
	Text2Pos [8]	11.8	24.6	32.5	8.6	18.1	24.0	3.3	7.8	11.0
	Text2Loc [21]	29.3	47.7	56.9	21.6	39.3	48.2	17.0	32.0	40.1
Baseline	MambaPlace [10]	31.0	52.0	62.0	-	-	-	-	-	-
	CMMLoc [11]	32.3	53.4	63.1	-	-	-	-	-	-
	Text2Loc++ (Ours)	35.3	57. 6	66.9	34.5	56.6	65.9	27.9	48.1	57.7
D (1)	Text2Pos [8]	10.5	21.8	28.7	8.0	17.5	23.6	3.3	8.0	11.4
Ketinement	Text2Loc [21]	29.0	48.8	58.0	21.3	39.7	48.6	18.0	34.2	42.4
	Text2Loc++ (Ours)	34.6	56.5	65.6	34.0	56.8	65.4	26.2	46.0	55.7
				Paris_CA						
	Text2Pos [8]	2.9	8.0	12.0	1.3	3.4	5.1	0.6	1.9	3.2
D 1:	Text2Loc [21]	11.2	21.2	28.5	6.0	14.1	20.1	2.5	5.4	8.6
Baseline	MambaPlace [10]	9.9	21.4	29.1	-	-	-	-	-	-
	CMMLoc [11]	12.5	25.6	33.3	- 10.0	- 05 5	- 22.6	-	- 01.0	- 27 F
	Text2Loc++ (Ours)	14.2	28.2	36.0	12.8	25.5	33.6	9.8	21.2	27.5
D - C t	Text2Pos [8]	6.0 23.9	15.1 44.9	22.2 55.6	3.8 12.9	9.4 29.1	13.2 37.8	1.8 11.5	5.7 24.5	8.8 33.1
Kennement	Text2Loc [21] Text2Loc++ (Ours)	23.9 28.4	51.6	62.5	12.9 27.2	29.1 49.9	60.3	11.5 18.5	36.7	33.1 46.4
	Text2Loc++ (Ours)	20.4	31.0			47.7	00.5	10.5	50.7	10.1
	T. (2D. [0]			Toront						
	Text2Pos [8]	2.1	6.3	9.6	1.9	5.7	8.7	0.8	2.1	3.4
Baseline	Text2Loc [21]	6.2	15.5	21.1	3.7	8.3	12.6	2.3	6.1	9.2
	MambaPlace [10] CMMLoc [11]	10.7 7.6	22.0 17.9	30.0	-	-	-	-	-	-
	Text2Loc++ (Ours)	13.2	26.4	24.1 34.6	13.2	25.7	33.8	10.6	21.3	27.4
	Text2Pos [8]	3.4	10.0	14.7	1.5	4.6	6.9	1.2	3.5	5.3
Refinement	Text2Loc [21]	15.6	31.5	39.2	7.8	18.0	25.7	2.5	16.6	22.7
	Text2Loc++ (Ours)	23.1	41.3	49.2	21.1	38.5	47.7	14.5	28.4	35.0
			Kľ	TTI360Pose	(no color) [8]				
	Text2Pos [8]	2.2	5.6	8.5	1.9	4.4	6.6	0.8	2.4	3.8
Baseline	Text2Loc [21]	7.7	16.4	22.3	3.0	7.2	10.4	2.4	5.7	8.6
	Text2Loc++ (Ours)	10.6	20.8	27.1	10.2	19.7	25.9	7.0	14.9	20.1
- 4	Text2Pos [8]	2.0	5.6	8.3	1.2	3.5	5.7	0.9	2.4	3.9
Refinement	Text2Loc [21]	7.7	16.7	22.7	3.1	7.2	10.4	2.4	6.1	9.2
	Text2Loc++ (Ours)	10.6	21.5	27.2	9.7	20.1	25.8	7.3	15.1	20.1
				TUM						
D 1:	Text2Pos [8]	5.4	14.3	21.2	7.0	15.7	20.8	2.1	9.4	13.9
Baseline	Text2Loc [21]	15.5	29.8	39.5	5.5	14.6	22.2	7.7	16.4	24.3
	Text2Loc++ (Ours) Text2Pos [8]	17.0 10.5	31.1	43.0	13.9 5.0	31.4	41.0	10.0	24.4	33.7 19.2
Refinement		23.5	24.1 46.6	38.2 57.5	5.0 15.4	16.3 31.6	24.8 41.3	4.6 11.8	12.6 25.2	35.4
	Text2Loc++ (Ours)	27.2	50.8	62.5	26.2	48.4	60.0	23.8	41.9	53.4
	· · · · · ·			Paris_Li	ille [15]					
	Text2Pos [8]	4.0	9.3	14.2	3.7	9.7	13.3	1.3	4.3	7.0
Baseline	Text2Loc [21]	5.9	14.8	21.2	4.4	10.7	15.5	3.1	8.2	10.8
	Text2Loc++ (Ours)	6.9	13.3	21.5	6.2	15.9	22.0	6.5	14.1	19.2
	Text2Pos [8]	4.7	12.8	19.8	4.4	12.2	17.3	1.9	6.9	11.2
Refinement	Text2Loc [21]	9.9	25.4	36.8	7.6	18.5	25.9	6.3	16.7	25.4
	Text2Loc++ (Ours)	13.1	26.3	35.6	14.1	26.3	38.7	9.5	23.6	33.4

TABLE 3: The evaluation results of the global place recognition. The "setting" column (baseline or refinement) indicates which datasets are used to train the network, as detailed in Table. 1. The terms simple, moderate, and complex refer to the linguistic complexity of the textual descriptions used during both training and testing.

5.2 Evaluation Criteria

Following [8], we use Retrieve Recall at Top k ($k \in \{1,3,5\}$) to evaluate text-submap global place recognition. The ground-truth submap is defined as the submap whose centroid coordinates are closest to the ground-truth location among all candidates. For a given text description, if the ground-truth submap appears within the top-k predicted submaps, the case is considered positive; otherwise,

it is negative. For assessing localization performance, we evaluate with respect to the top k retrieved candidates $(k \in \{1,5,10\})$ and report localization recall. Localization recall measures the proportion of successfully localized queries if their error falls below specific error thresholds, specifically $\epsilon < 5/10/15m$ by default. Table 3 and 4 shows the accuracy results for global place recognition and fine localization respectively.

				:	Localization R	ecall (%) - ϵ <	$5/10/15m^{-2}$	↑		
Setting	Method	Simple			Moderate			Complex		
		k=1	k=5	k=10	k=1	k=5	k=10	k=1	k=5	k=10
				KITTI	360Pose [8]					
	Text2Pos [8]	12/21/24	32/47/51	42/60/64	7/16/20	20/38/44	28/50/57	3/6/8	9/19/24	14/29/36
	Text2Loc [21]	34/47/50	61/74/76	71/83/85	28/39/43	54/67/70	65/77/80	14/29/34	33/56/61	42/67/72
Baseline	MambaPlace [10]	38/52/55	66/79/81	76/87/89	-	-	-	-	-	-
	CMMLoc [11]	39/53/56	67/80/82	77/87/89	-	-	-	-	-	-
	Text2Loc++ (Ours)	44/58/61	72/84/85	80/90/91	40/56/60	68/82/84	77/89/90	30/47/51	58/74/77	68/83/86
	Text2Pos [8]	12/19/23	30/45/50	41/58/63	7/14/18	20/37/43	28/50/56	3/6/9	9/20/25	15/30/37
Refinement	Text2Loc [21]	35/48/51	64/76/78	73/84/85	28/40/49	56/68/71	67/78/80	15/31/37	35/59/64	44/70/75
	Text2Loc++ (Ours)	40/56/60	67/82/84	76/89/90	38/55/59	66/82/84	75/89/90	27/45/50	54/72/76	64/82/84
				Paris_0	CARLA [12]					
	Text2Pos [8]	3/7/11	11/23/31	18/35/44	1/3/5	4/11/17	8/18/28	1/2/4	3/7/12	5/12/19
	Text2Loc [21]	12/20/26	24/44/52	41/59/64	8/16/20	23/36/42	32/48/54	2/5/7	7/16/23	12/25/33
Baseline	MambaPlace [10]	11/22/27	31/50/56	39/61/68	-	-	-	-	-	-
	CMMLoc [11]	14/25/30	34/51/57	44/63/ 69	-	-	-	-	-	-
	Text2Loc++ (Ours)	17/30/34	36/53/58	47/65/69	14/26/30	33/50/56	43/62/67	9/20/25	24/43/49	32/53/60
	Text2Pos [8]	6/14/20	22/40/49	33/54/63	3/8/13	11/24/33	17/36/47	1/5/8	7/18/27	13/29/41
Refinement	Text2Loc [21]	25/43/49	52/74/79	64/85/88	16/30/36	39/60/66	52/73/78	9/23/30	26/51/59	37/64/72
	Text2Loc++ (Ours)	33/51/55	63/81/84	75/90/92	31/47/52	60/78/82	70/88/91	18/34/41	43/65/79	55/76/82
				Tor	onto [13]					
	Text2Pos [8]	2/6/8	9/19/24	15/30/37	2/6/8	7/17/24	11/27/37	1/2/4	3/7/12	5/13/21
	Text2Loc [21]	10/16/19	24/39/44	34/54/59	5/11/14	17/27/33	25/39/47	2/6/9	7/19/27	13/30/41
Baseline	MambaPlace [10]	12/23/27	31/50/56	42/63/68	-	-	-	-	-	-
	CMMLoc [11]	9/17/22	28/43/50	41/59/65	-	-	-	-	-	-
	Text2Loc++ (Ours)	16/26/29	36/54/59	47/68/73	14/25/28	32/49/54	42/62/67	9/21/25	24/43/49	34/56/62
	Text2Pos [8]	4/9/13	15/28/35	23/41/50	1/4/7	6/15/22	11/25/33	1/4/6	4/12/17	8/19/27
Refinement	Text2Loc [21]	18/30/35	39/59/64	52/72/76	10/19/23	28/45/50	39/59/66	6/15/21	17/39/48	26/52/62
	Text2Loc++ (Ours)	30/43/46	57/69/72	68/81/84	26/39/42	51/67/71	63/78/82	15/30/35	36/57/62	47/69/74
				KITTI360Pc	ose (no color)	[8]				
	Text2Pos [8]	2/4/6	8/15/19	14/24/29	2/4/5	6/12/16	10/20/25	1/2/3	3/8/11	6/13/18
Baseline	Text2Loc [21]	8/12/13	23/32/35	33/45/48	3/5/7	11/17/21	17/26/30	2/4/5	7/14/17	11/21/26
	Text2Loc++ (Ours)	11/16/17	26/38/41	36/51/54	10/15/16	25/36/39	34/49/52	6/11/12	17/29/32	24/40/44
	Text2Pos [8]	2/4/6	8/16/19	14/25/30	1/2/4	5/10/14	8/16/22	1/2/3	3/7/10	6/13/17
Refinement	Text2Loc [21]	8/12/13	23/33/36	33/46/50	4/6/7	12/18/21	18/28/32	2/4/6	8/15/19	12/23/28
	Text2Loc++ (Ours)	10/16/17	26/38/41	36/51/54	10/15/16	24/36/39	33/49/52	6/11/12	17/29/32	24/40/44
				TU	JM [14]					
	Text2Pos [8]	5/14/20	19/41/55	29/57/73	6/13/20	16/34/47	25/50/61	1/6/13	10/24/41	17/37/56
Baseline	Text2Loc [21]	11/29/40	29/58/68	42/74/83	6/14/23	16/37/49	25/49/64	5/13/23	18/40/55	29/58/72
	Text2Loc++ (Ours)	12/30/39	31/59/68	47/76/83	9/28/35	26/59/65	39/74/82	8/19/26	26/51/59	40/68/76
	Text2Pos [8]	10/21/29	28/55/67	39/70/81	4/11/20	19/42/57	29/58/72	4/11/19	15/35/49	22/49/62
Refinement	Text2Loc [21]	25/44/52	54/79/83	68/89/91	15/32/41	37/66/74	52/80/86	9/21/32	30/54/64	41/70/80
	Text2Loc++ (Ours)	29/47/54	57/79/82	61/88/90	21/47/53	49/77/81	63/87/90	20/38/46	42/69/76	54/82/87
				Paris	_Lille [15]					
	Text2Pos [8]	3/9/14	12/30/41	21/47/61	3/10/15	10/28/40	18/43/55	1/4/8	5/16/25	12/29/41
Baseline	Text2Loc [21]	5 /12/ 18	16/ 36/46	28/55/65	4/11/17	12/28/39	20/44/59	2/5/9	9/21/31	14/35/48
	Text2Loc++ (Ours)	5/13/18	18 /34/ 46	30 /53/ 65	4/11/17	16/36/48	26/55/68	5/10/15	15/33/43	25/50/64
	Text2Pos [8]	5/11/17	16/54/45	28/53/65	4/10/15	12/32/43	21/50/63	1/7/12	8/26/36	17/42/53
Refinement	Text2Loc [21]	10/21/ 27	33/50/ 57	47/67/74	8/14/21	24/40/51	39/61/71	5/13/20	19/38/50	29/56/68
	Text2Loc++ (Ours)	12/22/ 26	35/51/57	51/70/77	11/22/25	34/53/59	48/71/77	8/16/20	27/48/58	38/69/77

TABLE 4: The evaluation results of the fine localization. The "setting" column (baseline or refinement) indicates which datasets are used to train the network, as detailed in Table. 1. The terms simple, moderate, and complex refer to the linguistic complexity of the textual descriptions used during both training and testing.

5.3 Results

We compare our proposed Text2Loc++ with several state-of-the-art methods: Text2Pos [8], RET [9], MambaPlace [10], and CMMLoc [11]. For completeness, we also include our previous version, Text2Loc [21], to highlight improvements. For a fair comparison, all methods are evaluated on six benchmark datasets for both global place recognition and fine-grained localization. We evaluate under two training settings: baseline and refinement, as detailed in Section 5.1.2 and Table 1. In addition, we analyze the model's performance under different levels of text complexity to assess robustness to linguistic variation.

5.3.1 Global Place Recognition

Baseline Networks. Text2Loc++ achieves the best performance on the KITTI360Pose test set, reaching a recall of 35.3% at top-1. Notably, this outperforms the recall achieved by the current state-of-the-art method CMMLoc by a wide margin of **9.3%**. Furthermore, Text2Loc++ achieves recall rates of 57.6% and 66.9% at top-3 and top-5, respectively, representing substantial improvements of 7.8% and 6.0% relative to the performance of CMMLoc. These improvements demonstrate the efficiency of our Text2Loc++ to capture local information from the cross-model and generate more discriminative global descriptors. More qualitative results are given in Section **7.1**. A horizontal comparison between

"color" and "no-color" input for the KITTI360Pose dataset shows that all models experience a significant performance drop, highlighting the importance of color information in the 3D localization task.

3D Generalization. To evaluate the generalization ability of our network, we train solely on the KITTI360Pose dataset and evaluate on other datasets, including Paris_CARLA [12], Toronto [13], TUM [14] and Paris [15] datasets. Excitingly, our network performs this task remarkably well. Across different datasets, we achieve strong results in top-1/3/5 recall, consistently outperforming all other models. Moreover, we observe that with color input, the model becomes more sensitive to variations in point cloud configurations, leading to larger performance differences across datasets.

Refinement Network. To further enhance generalization, we extend training beyond KITTI360Pose by incorporating additional datasets—Paris_CARLA (with color), and Lille and TUM (without color). As shown in Table 3, this refinement strategy significantly improves performance on previously unseen datasets, particularly Toronto (color) and Lille (no_color), demonstrating the effectiveness of our approach. Despite using only a small amount of additional data, Text2Loc++ achieves strong generalization across diverse domains in LiDAR-based place recognition. Notably, the inclusion of extra training data does not noticeably degrade performance on the original KITTI360Pose test set. These results highlight the robustness of our model and suggest that, with the availability of more diverse LiDAR datasets, further performance gains can be achieved—ultimately contributing to more consistent localization across varied environments.

Text Generalization. To assess the model's generalizability from a language perspective, we evaluate its performance across three levels of text complexity: simple, moderate, and complex. On the KITTI360Pose test set, the performance with moderate text input remains comparable to that with simple descriptions, suggesting that the model can effectively handle moderately complex language. However, performance degrades with complex inputs, indicating that challenges remain in filtering redundant information, extracting relevant content, and processing longer descriptions. On other datasets, the performance drop is more pronounced as text complexity increases. This suggests that the difficulty of cross-modal alignment in unfamiliar domains further limits the model's ability to interpret and leverage complex language.

5.3.2 Fine Localization

To enhance localization accuracy, prior works [8], [9] introduce a fine localization stage. For a fair comparison, we adopt the same training configuration as in [8], [9] for our fine localization network. As shown in Table 4, we report the top-k (k=1,5,10) recall rates under different error thresholds $\epsilon < 5/10/15$, m. On the KITTI360Pose (color) test set with simple text descriptions, Text2Loc++ achieves a top-1 recall rate of 44% under an error bound of $\epsilon < 5$, m, outperforming the previous state-of-the-art CMMLoc by 15%. Moreover, Text2Loc++ consistently maintains superior performance when the localization error tolerance is relaxed or when k increases. These results demonstrate that

C III	Submap	Submap Retrieval Recall (%) ↑				
Setting	k = 1	k = 3	k = 5			
w/o masked instance	32.1	53.5	62.6			
matching	10.1	21.3	28.5			
Text2Loc++	35.3	57.6	66.9			

TABLE 5: Performance analysis of the masked instance training. "matching" refers to retaining only the instances in the submaps that are explicitly described in the text instead of masked instance training.

C-11:	Submap Retrieval Recall (%) ↑				
Setting	k = 1	k = 3	k = 5		
w/o instance loss	33.2	54.9	64.0		
w/o text loss	33.4	56.2	65.3		
w/o submap loss	32.5	54.1	63.6		
Text2Loc++	35.3	57.6	66.9		

TABLE 6: Performance analysis of the each component of the proposed modality-aware hierarchical contrastive learning.

Text2Loc++ can more accurately interpret textual descriptions and achieve stronger semantic understanding of point clouds compared to prior methods. Qualitative examples are provided in Section 7.1. Text2Loc++ also achieves the best performance in the other datasets and refinement training. For different levels of text difficulty, moderate text descriptions show a slight performance drop compared to simple descriptions. Since fine localization requires more precise extraction of textual information than global place recognition, it is more sensitive to the complexity of the input text. With complex text input, the model struggles to accurately match the textual descriptions with the corresponding information in the submaps, leading to a noticeable decline in overall performance.

6 ABLATION STUDY

6.1 Ablation Study of Masked Instance Training

In Table 5, the removal of masked instance training results in an 8% decrease in model performance. Additionally, the complete exclusion of instances that not aligned with the textual descriptions substantially impairs the model's generalization capability. These observations underscore the efficacy of masked instance training in mitigating the challenges associated with many-to-many cross-modal alignment during the training process.

6.2 Ablation Study of Modality-aware Hierarchical Contrastive Learning

Table. 6 presents an ablation study evaluating the impact of different losses for the modality-aware hierarchical contrastive learning. We could conclude that removing any loss component leads to a drop in performance across all recall levels, highlighting the importance of each component to the model's overall effectiveness.

T1	TD	Extra	Submap	p Retrieval Recall (%) ↑		
Level	עו	EXITA	k = 1	k = 3	k=5	
	Х	-	22.7	41.8	50.8	
Moderate	Х	Shuffle	23.1	41.7	50.5	
	✓	-	34.0	56.8	65.4	
	Х	-	19.0	35.5	44.1	
	Х	Translate	16.7	31.8	39.8	
Complex	Х	TransLoRA*	29.9	50.5	59. 5	
-	✓	w/o LoRA	24.8	44.6	53.8	
	✓	-	<u>27.9</u>	<u>48.1</u>	<u>57.5</u>	

TABLE 7: Comparison of whether using text distillation for moderate and complex text on the KITTI360Pose benchmark. **TD** means text distillation. Several additional settings are applied during both training and testing phases. "Shuffle" involves randomizing the format of moderate descriptions. For a specific position, we utilize various formats of descriptions during training. "Translate" denotes the use of ChatGPT-4o [50] to simplify complex text descriptions before feeding them into the language encoder for both training and testing.

6.3 Ablation Study of Text Distillation

In Table 7, we report Text2Loc++ performance without the proposed Masked Instance Training (MIT), Modality-aware Hierarchical Contrastive Learning (MHCL), and the text distillation (TD), respectively, as well as the effect of different modules separately for different text types. In the simple text setting, we observe a steep drop in top-5 recall (from 63.5 to 57.2) when multiple alignment is disabled. However, limiting submaps to only the instances mentioned in the text does not improve performance; in fact, it makes it worse. The reason is that, during training, any extra instances are removed to perfectly match text and submap. In testing, though, submaps still include these extra instances, creating a mismatch between training and testing distributions and leading to the observed performance drop.

In both moderate and complex texts, we observe that disabling text distillation results in a decrease of 11% and 7% in top-5 performance, respectively. This highlights the critical role of text group alignment. Additionally, we find that modifying other modules cannot compensate for this loss. In the moderate setting, we attempted to increase the complexity of text during training by using linguistically diverse expressions conveying the same meaning. However, this approach did not lead to any performance improvement. This indicates that in the case of moderate text, the increased complexity prevents us from directly constructing a multimodal latent space. Therefore, the task must be divided: first, by constructing the latent space based on simple text, and then by using text distillation to map the complex text into the pre-established latent space. As shown in Table 3, even with the incorporation of MIT, MHCL, and TD, complex text input consistently yields approximately 10% lower performance than the simple input. As linguistic structures become more entangled and blended—with nonparallel syntax and the inclusion of irrelevant or extraneous content—the model exhibits difficulty in capturing all useful information. Although we initially consider applying text

	X7.1	Submap	Submap Retrieval Recall (%) ↑			
Parameter	Value	k = 1	k = 3	k = 5		
Loss	pairwise	31.5	53.3	62.5		
	dim = 64	28.3	48.5	57.4		
Latent Space	dim = 128	32.9	54.8	64.1		
	dim = 512	35.6	58.3	67.9		
	no HTM	31.0	51.0	59.8		
LITM I arrows	1 + 2	34.7	56.7	65.9		
HTM Layers	2 + 1	34.9	57.6	<u>66.9</u>		
	2 + 2	33.8	56.1	65.5		
Daalina	Intra Mean	35.0	57.5	66.4		
Pooling	Inter Mean	32.0	53.5	62.9		
	T5_base	34.1	56.8	65.5		
Backbones	T5_large	34.0	56.7	65.8		
(Text)	Llama3.2-1B	33.2	54.6	63.7		
(IEAU)	Llama3.2-3B	33.0	55.5	64.7		
	CLIP-B/16	33.2	54.6	63.7		
	no number	33.6	54.6	63.7		
Input Branches	no color	26.0	45.6	54.8		
	no position	21.0	40.1	49.8		
Default Config	-	<u>35.3</u>	<u>57.6</u>	66.9		

TABLE 8: Performance analysis of global place recognition in the different configurations in the simple text mode. The default config utilize InfoNCE loss [51], 256 latent space, HTM (intra = 1 + inter = 1), max pooling in intra and inter encoder, T5_large [16] backbones in the text module, and number, color, position branches.

simplification via ChatGPT-40 [50] to mitigate this issue, empirical results show no performance gain. A likely explanation is that the simplification process introduces semantic loss, which adversely affects model predictions. As discussed in Section 7.3, the model demonstrates high sensitivity to sentence-level content, where even minor omissions or distortions result in notable performance drops. Conversely, finetuning the T5 module with the LoRA method significantly enhances accuracy in the first stage. In the case of complex text descriptions, the best results are achieved using the translate-LoRA approach, where the finetuned T5 model first translates complex text into simplified text, which is then passed into our model. However, this method is approximately 10 times slower (~ 300 ms) than directly using the T5 encoder with LoRA (\sim 30 ms). Given the minimal performance difference and the substantial efficiency gain, we adopt the direct T5 encoder approach in our final model.

6.4 Analysis of Network Settings

The following ablation studies evaluate the effectiveness of different components of Text2Loc, including both the text-submap global place recognition and fine localization.

Global place recognition. In Table. 8, we assess the relative contribution of modules and settings.

We replace the InfoNCE loss [51] by pairwise ranking loss [52] that causes a slight decrease of the perforance.

By systematically varying the latent space dimension from 64 to 512, we find that when it is below 128, changes in dimensionality substantially influence the results. However, once the dimension exceeds 128, further increases have only a minor effect on performance. To ensure a fair comparison with other models, we set the dimension to 256 as our default setting.

We also explore the effect of hierarchical transformer modules (HTM). Removing the HTM layers altogether results in lower performance, whereas stacking layers (e.g., 1+2 or 2+1) introduces a minor alteration on the recall at all values.

We further study different pooling mechanisms for aggregating features, comparing intra- and inter-mean with the max pooling. The results suggest that intra-mean pooling performs on par with the default setting, while intermean pooling falls short.

Then, we investigate how different backbones affect the final results. Overall, we found that changing the backbone does not significantly alter submap retrieval recall. We tested an encoder-only T5 (since the T5 decoder component was not used in our model) and a decoder-only Llama. Even though Llama's architecture is more complex, it failed to improve performance on our task. The underlying reason is that our task requires precise extraction of linguistic information rather than broad understanding of multiple languages, and thus different LLM architectures performed similarly in this regard. Furthermore, we used the language encoder from CLIP [46] and found that the multimodal text encoder does not outperform a pure language model in our task.

Finally, we analyze the role of different input branches. Removing each branch leads to a noticeable drop in overall performance, emphasizing the importance of preserving all input modalities.

Our default configuration yields the highest recall, reflecting a balanced choice of loss function, latent dimension, HTM configuration, pooling strategy, backbone architecture, and input branches.

6.5 Ablation Study of Fine Localization

To analyze the effectiveness of each proposed module in our matching-free fine-grained localization, we separately evaluate the Cascaded Cross-Attention Transformer (CCAT) and Prototype-based Map Cloning (PMC) module, denoted as Text2Loc++_CCAT and Text2Loc++_PMC. For a fair comparison, all methods utilize the same submaps retrieved from our global place recognition. The results are shown in Table. 9. Text2Pos* significantly outperforms the origin results of Text2Pos [8], indicating the superiority of our proposed global place recognition. Notably, replacing the matcher in Text2Pos [8] with our CCAT results in about 10% improvements at top 1 on the test set. We also observe the inferior performance of Text2Loc++_PMC to the proposed method when interpreting only the proposed PMC module into the Text2Pos [8] fine localization network. The results are consistent with our expectations since PMC can lead to the loss of object instances in certain submaps. Combining both modules achieves the best performance, improving the performance by 10% at top 1 on the test set. This demonstrates adding more training submaps by PMC is beneficial for our matching-free strategy without any textinstance matches.

	Localizati	ion Recall (%	$(\delta) - \epsilon < 5m \uparrow$
Method	k = 1	k = 5	k = 10
Text2Pos [8]	12.2	31.9	43.0
Text2Pos*	36.6	64.7	72.8
Text2Loc++_PMC	36.8	64.6	72.9
Text2Loc++_CCAT	39.9	69.7	78.2
Text2Loc++ (Ours)	43.8	72.1	80.0

TABLE 9: Ablation study of the fine localization on the KITTI360Pose benchmark. * indicates the fine localization network from Text2Pose [8], and the submaps retrieved through our global place recognition. Text2Loc++_CCAT indicates the removal of only the PMC while retaining the CCAT in our network. Conversely, Text2Loc++_PMC keeps the PMC but replaces the CCAT with the text-instance matcher in Text2Pos.

7 DISCUSSION

7.1 Qualitative Analysis

To complement the quantitative analysis, Fig. 7 presents qualitative examples, showing two correct localizations and one failure case from text descriptions. Given a query text, we visualize the ground truth, the top-3 retrieved submaps, and the fine localization predictions. Within the text-submap global place recognition setting, a retrieved submap is defined as positive if it includes the target location. We provide text inputs with different levels of complexity across various scenes. Subfigures (a)-(c) correspond to simple, moderate, and complex text descriptions, respectively. The results allow us to intuitively observe how the model performs under different degrees of textual complexity. In most cases, Text2Loc++ effectively retrieves the ground-truth submap or spatially adjacent ones. Nonetheless, as shown in (b), some negative submaps may still appear among the top-3 retrieved candidates. By comparing (a) and (b), Text2Loc++ demonstrates its ability to predict more accurate locations by leveraging positively retrieved submaps during fine localization. With increasing text complexity, more failure cases like (c) occur, where all retrieved submaps are negative. In these cases, fine localization has difficulty predicting accurate positions, indicating its reliance on coarse localization.

Through the qualitative results obtained from text queries of varying complexity, we identify two key challenges in outdoor multimodal text-to-point-cloud retrieval. (1) Scene similarity. Negative submaps may contain instances visually similar to the ground truth due to the limited diversity of outdoor environments. This highlights the necessity of highly discriminative representations to effectively distinguish between submaps. (2) Text complexity. Highly complex text descriptions, even when containing sufficient location cues, can degrade localization performance because of their intricate linguistic structures and the presence of irrelevant information.

7.2 Computational Cost Analysis

In this section, we analyze the computational requirements of our two stage networks in terms of parameter count and

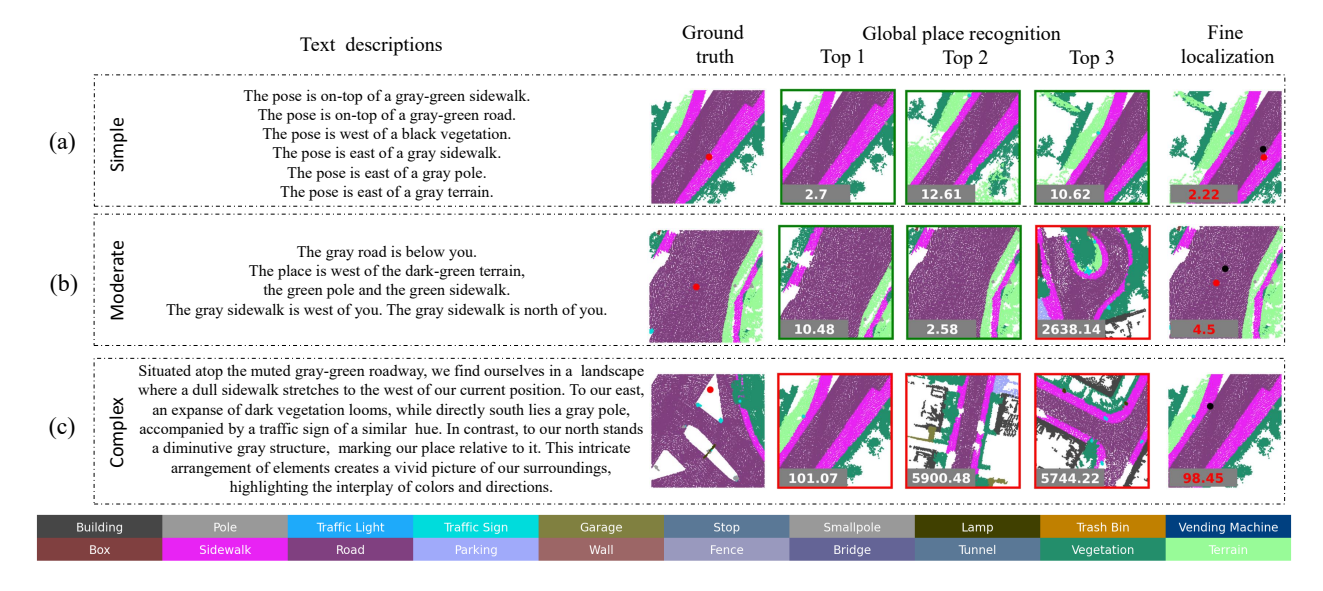


Fig. 7: Qualitative localization results on the KITTI360Pose dataset: In global place recognition, the numbers in top3 retrieval submaps represent center distances between retrieved submaps and the ground truth. Green boxes indicate positive submaps containing the target location, while red boxes signify negative submaps. For fine localization, red and black dots represent the ground truth and predicted target locations, with the red number indicating the distance between them. (a), (b), and (c) uses simple, moderate, and complex text descriptions respectively.

Method	Parameters (M)	Runtime (ms)	Localization Recall
Text2Loc++_Matcher	2.08	43.11	0.34
Text2Loc++ (Ours)	1.06	2.27	0.40

TABLE 10: Computational cost requirement analysis of our fine localization network on the KITTI360Pose test dataset.

time efficiency. For a fair comparison, all methods are evaluated on the KITTI360Pose test set using a single NVIDIA TITAN X (12 GB) GPU. In global recognition, Text2Loc++ requires 22.75 ms and 12.37 ms to generate global descriptors for a textual query and a submap, respectively, while Text2Pos [8] achieves this in 2.31 ms and 11.87 ms. The longer inference time for Text2Loc++ stems from the additional frozen T5 (30.21 ms with LoRA and 21.18 ms without LoRA) and HTM modules (1.57 ms). Our text and 3D encoders contain 13.65 M (excluding T5) and 1.84 M parameters, respectively. For fine localization, we substitute the proposed matching-free CCAT module with the text-instance matcher from [8], [9], denoted as Text2Loc++_Matcher. As shown in Table 10, Text2Loc++ is nearly twice as parameterefficient as previous works [8], [9] and requires only 5% of their inference time. This gain arises primarily because previous approaches employ SuperGlue [53] as a matcher, which is computationally heavy and time-consuming. Furthermore, our matching-free design eliminates the need for the Sinkhorn algorithm [54], further improving efficiency without sacrificing performance.

7.3 Robustness Analysis

In this section, we investigate the impact of text modifications on localization accuracy. To provide a comprehensive analysis, we systematically alter specific components of the query text—namely color, direction, and semantic class—at varying levels of severity. Specifically, we incrementally

Change Type	Hint
Original	The pose is east of a gray road.
Color	The pose is east of a green road.
Direction	The pose is west of a gray road.
Semantic class	The pose is east of a gray sidewalk.
Discard	(Sentence deleted)

TABLE 11: Change Instruction

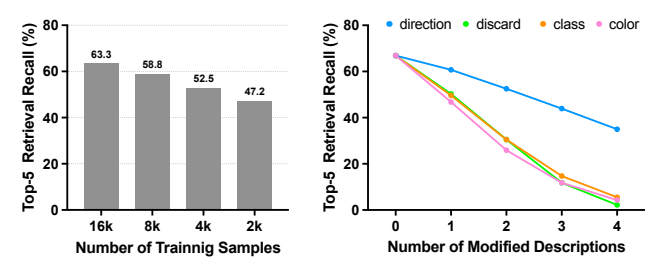


Fig. 8: Robustness analysis comparing different metrics.

modify between 1 and 5 sentences, ranging from minor to major changes. We also evaluate the network's robustness to erroneous versus missing information by randomly omitting sentences. Details of the modification strategies are provided in Table 11, and all evaluations are conducted on the KITTI360Pose test set. Results are illustrated in Fig. 8.

Our findings reveal that modifying or removing even a single sentence leads to a significant performance drop, particularly for changes involving color and semantic class. For example, altering just one sentence in these categories results in an approximate 30% decrease in both Top-1 and Top-5 recall, indicating that the network is highly sensitive to contextual text cues. In contrast, direction-related modifications (represented by the blue line) have the least impact on performance.

Further analysis shows that degradation patterns vary

across categories. Directional changes exhibit a near-linear decline with the number of modified sentences, while color and class modifications follow an exponential drop. Moreover, the impact of erroneous information—except for direction—is comparable to that of sentence omission, suggesting that incorrect context can be as detrimental as missing information. These results underscore the importance of robust context modeling in text-based localization systems.

We also assess robustness under reduced training data. Following the protocol in [55], we decrease the training set size from 16k to 2k samples. As shown in Fig. 8, Top-5 recall gradually drops from 63.3% to 47.2%, indicating that our model maintains strong retrieval performance even under significant data scarcity. While some degradation is expected, the relatively smooth decline demonstrates the model's resilience to limited supervision.

7.4 Embedding Space Analysis

To illustrate the structure of the learned embedding space, we visualize it using T-SNE [56], as presented in Fig. 9. The baseline method Text2Loc [21], not using masked instance training (MIT), modality-aware hierarchical contrastive learning (MHCL), and the text distillation (TD), results in a less discriminative embedding space, where positive submaps tend to lie far from their corresponding query text descriptions and are often dispersed across the space. At the same time, they also cause text embeddings with different expressions but the same meaning, as well as subsets of positive submaps (submaps containing only a subset of instances from the original submaps), to have a large distance from the original submaps. This negatively affects our ability to accurately perform text-based submap retrieval during testing. In contrast, the method with MIT, MHCL, TD brings positive submaps, subset of positive submaps, and query text representations significantly closer together within the embedding distance. It shows that the proposed network indeed results in a more discriminative cross-model space for recognizing places.

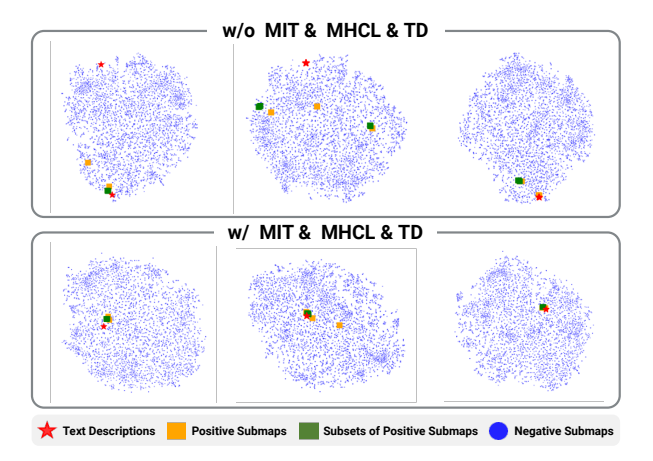


Fig. 9: T-SNE illustration comparison between with and without masked instance training (MIT), modality-aware hierarchical contrastive learning (MHCL), and text distillation (TD).

8 Conclusion

In this work, we address the under-explored problem of localizing 3D point cloud submaps from natural language descriptions, a key step toward more intuitive and flexible human-robot spatial interaction. We propose Text2Loc++, a novel coarse-to-fine framework that captures fine-grained semantic context across modalities. For global place recognition, we introduce an attention-based language encoder and a modality-aware hierarchical contrastive learning strategy with masked instance training to better align text and submaps. To handle complex language inputs, we incorporate text distillation and LoRA-based tuning. Furthermore, we are the first to propose a matching-free fine localization design, which is lighter, faster, and more accurate. Extensive experiments demonstrate that Text2Loc++ outperforms prior methods and generalizes well across diverse linguistic and geometric inputs. We hope this work inspires future research in language-grounded 3D localization and humancentric spatial understanding.

Acknowledgements. This work was supported by the ERC Advanced Grant SIMULACRON, by the Munich Center for Machine Learning, and by the Royal Academy of Engineering (RF\201819\18\163), by the Anhui Provincial Natural Science Foundation (2508085MF142). Some figures created by https://BioRender.com.

REFERENCES

- [1] Z. Min, B. Zhuang, S. Schulter, B. Liu, E. Dunn, and M. Chandraker, "Neurocs: Neural nocs supervision for monocular 3d object localization," in *Proceedings of the IEEE/CVF Conference on Computer Vision and Pattern Recognition (CVPR)*, June 2023, pp. 21404–21414. 1
- [2] P.-E. Sarlin, D. DeTone, T.-Y. Yang, A. Avetisyan, J. Straub, T. Malisiewicz, S. R. Bulò, R. Newcombe, P. Kontschieder, and V. Balntas, "Orienternet: Visual localization in 2d public maps with neural matching," in *Proceedings of the IEEE/CVF Conference on Computer Vision and Pattern Recognition (CVPR)*, June 2023, pp. 21 632–21 642.
- [3] Y. Hu, J. Yang, L. Chen, K. Li, C. Sima, X. Zhu, S. Chai, S. Du, T. Lin, W. Wang, L. Lu, X. Jia, Q. Liu, J. Dai, Y. Qiao, and H. Li, "Planning-oriented autonomous driving," in *Proceedings of the IEEE/CVF Conference on Computer Vision and Pattern Recognition*, 2023. 1
- [4] Y. Xia, Q. Wu, W. Li, A. B. Chan, and U. Stilla, "A lightweight and detector-free 3d single object tracker on point clouds," *IEEE Transactions on Intelligent Transportation Systems*, 2023. 1
- [5] Y. Xia, Y. Xu, C. Wang, and U. Stilla, "Vpc-net: Completion of 3d vehicles from mls point clouds," *ISPRS Journal of Photogrammetry* and Remote Sensing, vol. 174, pp. 166–181, 2021. 1
- [6] Y. Xia, M. Gladkova, R. Wang, Q. Li, U. Stilla, J. a. F. Henriques, and D. Cremers, "Casspr: Cross attention single scan place recognition," in *Proceedings of the IEEE/CVF International Conference on Computer Vision (ICCV)*, October 2023, pp. 8461–8472. 1, 3, 7
- [7] Y. Xia, "Perception of vehicles and place recognition in urban environment based on mls point clouds," Ph.D. dissertation, Technische Universität München, 2023. 1
- [8] M. Kolmet, Q. Zhou, A. Ošep, and L. Leal-Taixé, "Text2pos: Text-to-point-cloud cross-modal localization," in *Proceedings of the IEEE/CVF Conference on Computer Vision and Pattern Recognition*, 2022, pp. 6687–6696. 1, 2, 3, 4, 6, 7, 8, 10, 11, 12, 14, 15
- [9] G. Wang, H. Fan, and M. Kankanhalli, "Text to point cloud localization with relation-enhanced transformer," arXiv preprint arXiv:2301.05372, 2023. 1, 3, 4, 6, 7, 11, 12, 15
- [10] T. Shang, Z. Li, P. Xu, and J. Qiao, "Mambaplace:text-to-point-cloud cross-modal place recognition with attention mamba mechanisms," 2025. [Online]. Available: https://arxiv.org/abs/2408.15740 1, 3, 10, 11

- [11] Y. Xu, H. Qu, J. Liu, W. Zhang, and X. Yang, "Cmmloc: Advancing text-to-pointcloud localization with cauchy-mixturemodel based framework," 2025. [Online]. Available: https://arxiv.org/abs/2503.02593 1, 3, 10, 11
- [12] J.-E. Deschaud, D. Duque, J. P. Richa, S. Velasco-Forero, B. Marcotegui, and F. Goulette, "Paris-carla-3d: A real and synthetic outdoor point cloud dataset for challenging tasks in 3d mapping," *Remote Sensing*, vol. 13, no. 22, 2021. [Online]. Available: https://www.mdpi.com/2072-4292/13/22/4713 1, 7, 10, 11, 12
- [13] W. Tan, N. Qin, L. Ma, Y. Li, J. Du, G. Cai, K. Yang, and J. Li, "Toronto-3D: A large-scale mobile lidar dataset for semantic segmentation of urban roadways," in *Proceedings of the IEEE/CVF Conference on Computer Vision and Pattern Recognition Workshops*, 2020, pp. 202–203. 1, 7, 10, 11, 12
- [14] J. Zhu, J. Gehrung, R. Huang, B. Borgmann, Z. Sun, L. Hoegner, M. Hebel, Y. Xu, and U. Stilla, "Tum-mls-2016: An annotated mobile lidar dataset of the tum city campus for semantic point cloud interpretation in urban areas," *Remote Sensing*, vol. 12, no. 11, p. 1875, 2020. 1, 7, 10, 11, 12
- [15] X. Roynard, J.-E. Deschaud, and F. Goulette, "Paris-lille-3d: A large and high-quality ground-truth urban point cloud dataset for automatic segmentation and classification," The International Journal of Robotics Research, vol. 37, no. 6, pp. 545–557, 2018. 1, 7, 10, 11, 12
- [16] C. Raffel, N. Shazeer, A. Roberts, K. Lee, S. Narang, M. Matena, Y. Zhou, W. Li, and P. J. Liu, "Exploring the limits of transfer learning with a unified text-to-text transformer," *Journal of Machine Learning Research*, vol. 21, no. 140, pp. 1–67, 2020. [Online]. Available: http://jmlr.org/papers/v21/20-074.html 2, 4, 6, 13
- [17] X. Yuan, Z. Lin, J. Kuen, J. Zhang, Y. Wang, M. Maire, A. Kale, and B. Faieta, "Multimodal Contrastive Training for Visual Representation Learning," in 2021 IEEE/CVF Conference on Computer Vision and Pattern Recognition (CVPR), Jun. 2021. 2
- [18] Z. Wang, Y. Zhao, X. Cheng, H. Huang, J. Liu, L. Tang, L. Li, Y. Wang, A. Yin, Z. Zhang, and Z. Zhao, "Connecting multi-modal contrastive representations," 2023. 2
- [19] J. E. Hu, Y. Shen, P. Wallis, Z. Allen-Zhu, Y. Li, S. Wang, and W. Chen, "Lora: Low-rank adaptation of large language models," *ArXiv*, vol. abs/2106.09685, 2021. [Online]. Available: https://api.semanticscholar.org/CorpusID:235458009 2, 6
- https://api.semanticscholar.org/CorpusID:235458009 2, 6
 [20] S. Xu, X. Li, H. Yuan, L. Qi, Y. Tong, and M.-H. Yang, "Llavadi: What matters for multimodal large language models distillation," 2024. [Online]. Available: https://arxiv.org/abs/2407.19409 2
- [21] Y. Xia, L. Shi, Z. Ding, J. F. Henriques, and D. Cremers, "Text2loc: 3d point cloud localization from natural language," in *Proceedings* of the IEEE/CVF Conference on Computer Vision and Pattern Recognition, 2024. 3, 10, 11, 16
- [22] D. G. Lowe, "Distinctive image features from scale-invariant keypoints," *International journal of computer vision*, vol. 60, pp. 91–110, 2004.
- [23] E. Rublee, V. Rabaud, K. Konolige, and G. Bradski, "Orb: An efficient alternative to sift or surf," in 2011 International conference on computer vision. Ieee, 2011, pp. 2564–2571.
- [24] P.-E. Sarlin, C. Cadena, R. Siegwart, and M. Dymczyk, "From coarse to fine: Robust hierarchical localization at large scale," in *Proceedings of the IEEE/CVF Conference on Computer Vision and Pattern Recognition*, 2019, pp. 12716–12725. 3
- [25] T. Sattler, B. Leibe, and L. Kobbelt, "Efficient & effective prioritized matching for large-scale image-based localization," *IEEE transac*tions on pattern analysis and machine intelligence, vol. 39, no. 9, pp. 1744–1756, 2016. 3
- [26] M. Angelina Uy and G. Hee Lee, "Pointnetvlad: Deep point cloud based retrieval for large-scale place recognition," in *Proceedings* of the IEEE Conference on Computer Vision and Pattern Recognition, 2018, pp. 4470–4479.
- [27] Y. Xia, Y. Xu, S. Li, R. Wang, J. Du, D. Cremers, and U. Stilla, "Soenet: A self-attention and orientation encoding network for point cloud based place recognition," in *Proceedings of the IEEE/CVF Conference on computer vision and pattern recognition*, 2021, pp. 11348–11357. 3, 5
- [28] Z. Zhou, C. Zhao, D. Adolfsson, S. Su, Y. Gao, T. Duckett, and L. Sun, "Ndt-transformer: Large-scale 3d point cloud localisation using the normal distribution transform representation," in 2021 IEEE International Conference on Robotics and Automation (ICRA). IEEE, 2021, pp. 5654–5660.

- [29] H. Deng, T. Birdal, and S. Ilic, "Ppfnet: Global context aware local features for robust 3d point matching," in *Proceedings of the IEEE Conference on Computer Vision and Pattern Recognition*, 2018, pp. 195–205.
- [30] Z. Fan, Z. Song, H. Liu, Z. Lu, J. He, and X. Du, "Svt-net: Super light-weight sparse voxel transformer for large scale place recognition." AAAI, 2022. 3
- [31] W. Zhang, H. Zhou, Z. Dong, Q. Yan, and C. Xiao, "Rank-pointretrieval: Reranking point cloud retrieval via a visually consistent registration evaluation," *IEEE Transactions on Visualization and Computer Graphics*, 2022. 3
- [32] J. Ma, J. Zhang, J. Xu, R. Ai, W. Gu, and X. Chen, "Overlaptransformer: An efficient and yaw-angle-invariant transformer network for lidar-based place recognition," *IEEE Robotics and Automation Letters*, vol. 7, no. 3, pp. 6958–6965, 2022. 3
- [33] T. Barros, L. Garrote, R. Pereira, C. Premebida, and U. J. Nunes, "Attdlnet: Attention-based deep network for 3d lidar place recognition," in *Iberian Robotics conference*. Springer, 2022, pp. 309–320.
- [34] J. Ma, G. Xiong, J. Xu, and X. Chen, "Cvtnet: A cross-view transformer network for place recognition using lidar data," arXiv preprint arXiv:2302.01665, 2023. 3
- [35] J. Komorowski, "Minkloc3d: Point cloud based large-scale place recognition," in Proceedings of the IEEE/CVF Winter Conference on Applications of Computer Vision, 2021, pp. 1790–1799.
- [36] T.-Y. Lin, P. Dollár, R. Girshick, K. He, B. Hariharan, and S. Belongie, "Feature pyramid networks for object detection," in Proceedings of the IEEE Conference on Computer Vision and Pattern Recognition, 2017, pp. 2117–2125.
- [37] F. Radenović, G. Tolias, and O. Chum, "Fine-tuning cnn image retrieval with no human annotation," *IEEE Transactions on Pattern Analysis and Machine Intelligence*, vol. 41, no. 7, pp. 1655–1668, 2018.
- [38] A. Segal, D. Haehnel, and S. Thrun, "Generalized-icp." in *Robotics: science and systems*, vol. 2, no. 4. Seattle, WA, 2009, p. 435. 3
- [39] G. Elbaz, T. Avraham, and A. Fischer, "3d point cloud registration for localization using a deep neural network auto-encoder," in Proceedings of the IEEE conference on computer vision and pattern recognition, 2017, pp. 4631–4640.
- [40] M. Prabhudesai, H.-Y. F. Tung, S. A. Javed, M. Sieb, A. W. Harley, and K. Fragkiadaki, "Embodied language grounding with implicit 3d visual feature representations," 2019. 3
- [41] P. Achlioptas, A. Abdelreheem, F. Xia, M. Elhoseiny, and L. Guibas, "Referit3d: Neural listeners for fine-grained 3d object identification in real-world scenes," in Computer Vision–ECCV 2020: 16th European Conference, Glasgow, UK, August 23–28, 2020, Proceedings, Part I 16. Springer, 2020, pp. 422–440. 3
- [42] D. Z. Chen, A. X. Chang, and M. Nießner, "Scanrefer: 3d object localization in rgb-d scans using natural language," in European conference on computer vision. Springer, 2020, pp. 202–221.
- [43] Z. Yuan, X. Yan, Y. Liao, R. Zhang, S. Wang, Z. Li, and S. Cui, "Instancerefer: Cooperative holistic understanding for visual grounding on point clouds through instance multi-level contextual referring," in *Proceedings of the IEEE/CVF International Conference on Computer Vision*, 2021, pp. 1791–1800.
- [44] M. Feng, Z. Li, Q. Li, L. Zhang, X. Zhang, G. Zhu, H. Zhang, Y. Wang, and A. Mian, "Free-form description guided 3d visual graph network for object grounding in point cloud," in *Proceedings* of the IEEE/CVF International Conference on Computer Vision, 2021, pp. 3722–3731. 3
- [45] C. R. Qi, L. Yi, H. Su, and L. J. Guibas, "Pointnet++: Deep hierarchical feature learning on point sets in a metric space," Advances in neural information processing systems, vol. 30, 2017. 4
- [46] A. Radford, J. W. Kim, C. Hallacy, A. Ramesh, G. Goh, S. Agarwal, G. Sastry, A. Askell, P. Mishkin, J. Clark et al., "Learning transferable visual models from natural language supervision," in *International conference on machine learning*. PMLR, 2021, pp. 8748–8763. 6, 14
- [47] Y. Liao, J. Xie, and A. Geiger, "KITTI-360: A novel dataset and benchmarks for urban scene understanding in 2d and 3d," arXiv preprint arXiv:2109.13410, 2021. 7
- [48] M. Cordts, M. Omran, S. Ramos, T. Rehfeld, M. Enzweiler, R. Benenson, U. Franke, S. Roth, and B. Schiele, "The cityscapes dataset for semantic urban scene understanding," in *Proc. of the IEEE Conference on Computer Vision and Pattern Recognition (CVPR)*, 2016.

- [49] OpenAI, "Gpt-4 technical report," 2024. [Online]. Available:
- https://arxiv.org/abs/2303.08774 9
 —, "Gpt-4o system card," 2024. [Online]. Available: https: //arxiv.org/abs/2410.21276 13
- [51] A. van den Oord, Y. Li, and O. Vinyals, "Representation learning with contrastive predictive coding," 2019. [Online]. Available: https://arxiv.org/abs/1807.03748 13
- [52] R. Kiros, R. Salakhutdinov, and R. S. Zemel, "Unifying visualsemantic embeddings with multimodal neural language models," 2014. [Online]. Available: https://arxiv.org/abs/1411.2539 13
- [53] P.-E. Sarlin, D. DeTone, T. Malisiewicz, and A. Rabinovich, "SuperGlue: Learning feature matching with graph neural networks," in CVPR, 2020. [Online]. Available: https://arxiv.org/ abs/1911.11763 15
- "Sinkhorn distances: [54] M. Cuturi, Lightspeed computation of optimal transport," in Advances in Information Processing Systems, C. Burges, L. Bottou, M. Welling, Z. Ghahramani, and K. Weinberger, Eds., vol. 26. Curran Associates, Inc., 2013. [Online]. Available: https://proceedings.neurips.cc/paper_files/paper/2013/file/af21d0c97db2e27e13572cbf59eb343d-Paper.pdf 15
- [55] K. Zha, P. Cao, J. Son, Y. Yang, and D. Katabi, "Rank-n-contrast: Learning continuous representations for regression," in Thirtyseventh Conference on Neural Information Processing Systems, 2023.
- [56] L. Van der Maaten and G. Hinton, "Visualizing data using t-sne." *JMLR*, 2008. 16



João F. Henriques is a Research Fellow of the Royal Academy of Engineering, working at the Visual Geometry Group (VGG) at the University of Oxford. His research focuses on computer vision and deep learning, with the goal of making machines more perceptive, intelligent and capable of helping people. He created the KCF and SiameseFC visual object trackers, which won the highly competitive VOT Challenge twice, and are widely deployed in consumer hardware, from Facebook apps to commercial drones. His

research spans many topics: robot mapping and navigation, including reinforcement learning and 3D geometry; multi-agent cooperation and "friendly" AI; as well as various forms of learning, from self-supervised, causal, and meta-learning, including optimisation theory.



Yan Xia is now a tenure-track Associate Professor at University of Science and Technology of China (USTC). He was a senior researcher in the Chair of Computer Vision and Artificial Intelligence at Technical University of Munich (TUM) and a research scientist at Munich Center for Machine Learning (MCML), working with Prof. Daniel Cremers. He obtained his PhD degree from TUM in 2023 and was a visiting scholar in Visual Geometry Group (VGG) at University of Oxford. His research interests include 3D vision,

robotics, and autonomous driving.



Daniel Cremers is a Professor at TUM, where he is holding the Chair of Computer Vision and Artificial Intelligence. He is also a co-founder of Artisense, a deep-tech startup developing computer vision and AI solutions for robotics and autonomous driving. Daniel has served as an area chair for ICCV, ECCV, CVPR, ACCV, IROS, etc., and as a program chair for ACCV 2014. In 2018, he was an organizer of ECCV in Munich. His publications received several awards and have been cited more than 70000 times. In

2016, Daniel received the Leibniz Award, the biggest award in German academia.



Letian Shi is currently a master's student in Operations Research at the Technical University of Munich (TUM). He obtained his M.Sc. degree in Data Engineering and Analytics from TUM in 2023. His research interests include 3D vision, multimodal model, and 3D generation.



Yilin Di is currently a PhD researcher at the Technical University of Munich (TUM), working under the supervision of Prof. Henrik Semb. She previously worked as a research scientist at the Helmholtz Zentrum München (HMGU). She obtained her master's degree from TUM in 2021. Her research interests include 3D cell models, organoid development, and live imaging.